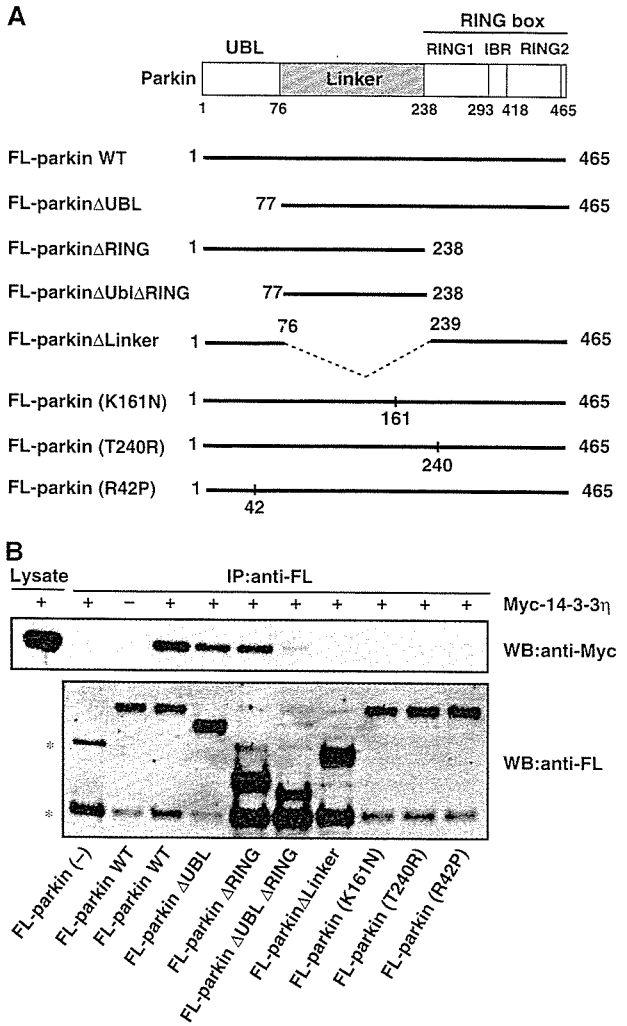

Figure 2 Domain analysis of the parkin region that interacts with 14-3-3η. (**A**) Schematic representation of WT parkin and its deletion- and disease-related missense mutants. See text for the domain structures of parkin and mutants. The dotted line denotes the deleted region. (**B**) Interaction between 14-3-3η and parkin mutants. FL-parkin (2 μg) or its mutant (10 μg) plasmids were transfected into HEK293 cells, as described in Figure 1D. The cell lysates (200–600 μl) were immunoprecipitated with anti-FL-antibody beads. Note that various amounts of the lysates were used to adjust roughly the levels of expressed parkin mutants. The resulting immunoprecipitates were mixed with other cell lysates (200 μl) prepared from cells that had been transfected with Myc-14-3-3η plasmid (2 μg) and incubated for 6 h at 4°C. Then, the extensively washed immunoprecipitates and cell lysate (7.5% input) were analyzed by Western blotting with anti-Myc and FL antibodies. Asterisks denote nonspecific bands.

The full-length parkin could bind 14-3-3η. Deletion of either UBL or RING-box domain reduced the binding compared to the full-length parkin, although these deletion mutants retained the ability to bind to 14-3-3η. Furthermore, mutants with combined deletions of the UBL and RING-box domains, that is, the linker region, could also bind 14-3-3η to a lesser extent. Conversely, deletion of the linker region resulted in the loss of ability to bind 14-3-3η. Taken together, it is concluded that the linker region is necessary for the interaction between parkin and 14-3-3η, although the UBL and RING-box domains may enhance the binding affinity.

Interestingly, the ARJP disease-causing missense mutation within the linker region, that is, parkin(K161N), in which the Lys residue at position 161 was replaced by Asn residue, showed complete loss of binding to 14-3-3η, confirming the importance of the linker region in the interaction between 14-3-3η and parkin. Unexpectedly, other disease-causing missense mutations of the UBL region, parkin(R42P), and the RING1 region, parkin(T240R), also showed complete loss of interaction with 14-3-3η (Figure 2). Thus, although the UBL and RING-box domains are not primarily required for the binding, both R42P and T240R mutations in the UBL and RING-box domains, respectively, deleteriously affect the neighboring linker domain. Alternatively, since 14-3-3 is known to form a homo- or hetero-dimer, and thus has two binding sites (Aitken *et al*, 2002), it is plausible that 14-3-3η interacts with two distinct regions of parkin, one major site of which is the linker region.

Effect of suppression of 14-3-3η on parkin E3 activity

We next investigated the role of parkin–14-3-3η binding on parkin activity. At first, we tested its effect on the ubiquitin ligase activity of parkin. We incubated recombinant His-parkin with ubiquitin, E1, and E2 (UbcH7) *in vitro*. Under this condition, His-parkin appeared as a smear band, which likely reflects self-ubiquitylation (Figure 3A). Addition of recombinant GST-14-3-3η (Figure 3A, left panel) or untagged 14-3-3η (Figure 3A, right panel) to the reaction reduced the smear of His-parkin, and such reduction was proportionate to the added amount of GST-14-3-3η or 14-3-3η and resulted in the recovery of His-parkin of intact size. In addition, we found that 14-3-3η had no effect on the ubiquitylating activity of phosphorylated IκBα by a fully *in vitro* reconstituted system, containing E1, E2 (Ubc4), and E3 (the $SCF^{\beta TrCP}$ complex; Kawakami *et al*, 2001), indicating that 14-3-3η does not interfere with ubiquitylating reactions in general (data not shown). These results strongly suggest that 14-3-3η suppresses the intrinsic self-ubiquitylation activity of parkin.

We next tested whether 14-3-3η also affects the ubiquitylation activity of parkin in HEK293 cells. First, we examined the self-ubiquitylation of parkin, whose activity was observed by cotransfections of HA-ubiquitin and FL-parkin. Myc-14-3-3η almost completely suppressed the self-ubiquitylation activity of parkin, while Myc-14-3-3σ, β, and ζ had no inhibitory effect (Figure 3B), indicating the specific role of 14-3-3η for parkin. Second, we examined the effect of 14-3-3η on the ubiquitylation of a model substrate for parkin. When V5-tagged synphilin-1, a known parkin substrate (Chung *et al*, 2001), was transfected with FL-parkin and HA-ubiquitin in the cells, V5-synphilin-1 was found in ubiquitylated form, as demonstrated by the poly-ubiquitin chain formation (detected by anti-HA antibody) in anti-V5 immunoprecipitant (Figure 3C, top panel). V5-synphilin-1 was not ubiquitylated when FL-parkin was not cotransfected, suggesting that this ubiquitylation is mediated by coexpressed FL-parkin. Indeed, FL-parkin was found to be associated with V5-synphilin-1, further supporting the above notion (Figure 3C, second panel from the top). Note that the polyubiquitylated bands observed as the smear profile were considered to include not only major synphilin-1 bands over 90-kDa size but also self-ubiquitylated bands of parkin over 52-kDa size.

In the next step, we tested the effects of 14-3-3η on the ubiquitylation and binding activities of parkin to

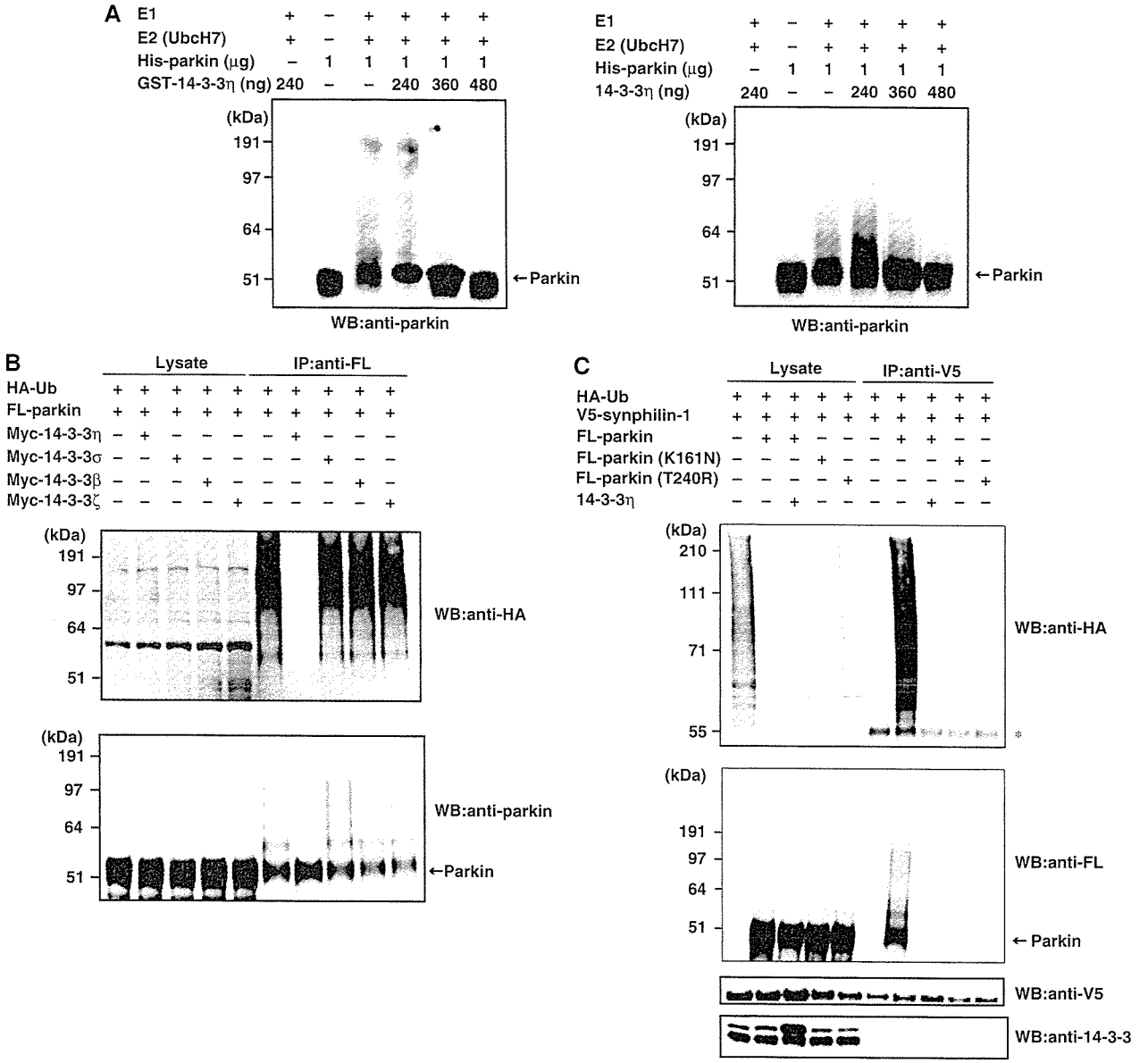

Figure 3 Effects of 14-3-3η on the E3 activity of parkin. (**A**) *In vitro* autoubiquitylation. The ubiquitylating assay was conducted as described in Materials and methods with or without various amounts of GST-14-3-3η (left panel) or 14-3-3η (right panel). After incubation, the reaction mixtures were subjected to SDS–PAGE, followed by Western blotting with anti-parkin. Arrow on the right indicates the position of His-parkin. (**B**) *In vivo* autoubiquitylation. HA-Ub (3 μg), FL-parkin (3 μg), and Myc-14-3-3η, σ, β, or ζ (6 μg) plasmids were transfected for 48 h into HEK293 cells as indicated. After immunoprecipitation with anti-FL, Western blotting was performed using antibodies against HA and parkin. Western blotting of all lysates was performed to test the expression levels (Lysate). (**C**) Ubiquitylation of synphilin-1 in HEK293 cells. HA-Ub (2 μg), FL-parkin (3 μg), FL-parkin(K161N) (3 μg), FL-parkin(T240R) (3 μg), Myc-14-3-3η (6 μg), and V5-synphilin-1 (4 μg) plasmids were transfected into HEK293 cells as in (B) at the indicated combinations. After immunoprecipitation with anti-V5 antibody, Western blotting was performed using antibodies against HA, FL, V5, and 14-3-3. Asterisk denotes an IgG heavy chain.

V5-synphilin-1. Cotransfection of 14-3-3η resulted in almost complete inhibition of the ubiquitylation of synphilin-1 by parkin and/or self-ubiquitylation of parkin (Figure 3C, top and second panels), as well as inhibition of the interaction between synphilin-1 and parkin (Figure 3C, second panel). 14-3-3η did not interact with synphilin-1 (Figure 3C, bottom panel). Taken together, these results suggest that 14-3-3η does not only inhibit the intrinsic ubiquitylation activity of parkin, but also its binding activity to the substrate and its ubiquitylation.

The ARJP disease-related parkin(K161N) and parkin(T240R) mutants, which cannot bind with 14-3-3η, could not bind and ubiquitylate synphilin-1 and/or self-ubiquitylation of parkin even in the absence of 14-3-3η (Figure 3C, top panel). Hence, the linker and RING-box domains of parkin are essential not only for the negative regulation by 14-3-3η, but also for the substrate recognition and ubiquitin-ligase activity. These results illustrate the importance of these regions of parkin on its positive and negative regulation.

Since parkin is known to associate with E2 (Shimura *et al*, 2000), we also examined the effect of 14-3-3η on the ability of parkin to recruit E2. For this purpose, we coexpressed HA-parkin with FL-UbcH7 or FL-Ubc7, both of which are known

to bind to parkin (Shimura *et al* 2000; Imai *et al*, 2001). Almost the same amounts of UbcH7 (Figure 4A) and Ubc7 (Figure 4B) were detected in the anti-parkin immunoprecipitants irrespective of cotransfection with Myc-14-3-3η. These findings indicate that 14-3-3η does not influence the recruitment of E2, that is, UbcH7 or Ubc7, to parkin.

α-Synuclein abrogates 14-3-3η-related parkin inactivation

Based on the above findings, we next examined the mechanism that regulates the 14-3-3η–parkin binding. As α-SN partly has a high homology to 14-3-3 isoforms (Ostrerova *et al*, 1999), we tested the effects of α-SN on the 14-3-3η-induced suppression of parkin. By cotransfection experiments in HEK293 cells, parkin again ubiquitylated synphilin-1, and 14-3-3η inhibited the parkin-mediated ubiquitylation (Figure 5A). Coexpression of α-SN resulted in the recovery of ubiquitylation of synphilin-1 and the association of synphilin-1 with parkin, suggesting that α-SN abrogates the 14-3-3η-induced suppression of parkin (Figure 5A, top panel). Importantly, the familial PD-related mutants of α-SN(A30P) (Kruger *et al*, 1998) and α-SN(A53T) (Polymeropoulos *et al*, 1997) could not abrogate the inhibitory role of 14-3-3η. Similar results were observed by detection of self-ubiquitylation activity of parkin (Figure 5A, second panel).

We then tested whether α-SN can release the binding of Myc-14-3-3η from parkin in cotransfection experiment. As shown in Figure 5B (top panel), FL-parkin was self-ubiquitylated in the absence of 14-3-3η. Coexpression of 14-3-3η inhibited the self-ubiquitylation of parkin, and this was accompanied by the binding of 14-3-3η to FL-parkin. Coexpression of α-SN abrogated the binding of 14-3-3η to parkin and resulted in the recovery of self-ubiquitylation of parkin. These effects were not seen by coexpression of α-SN(A30P) and α-SN(A53T) (Figure 5B, top panel). In addition, while the 14-3-3η–parkin interaction was considerably reduced by α-SN, it was not reduced by α-SN(A30P) or α-SN(A53T) (Figure 5B, bottom panel). Taken together, α-SN, but not α-SN(A30P) or α-SN(A53T), binds strongly to 14-3-3η and thereby releases parkin from the parkin–14-3-3η complex.

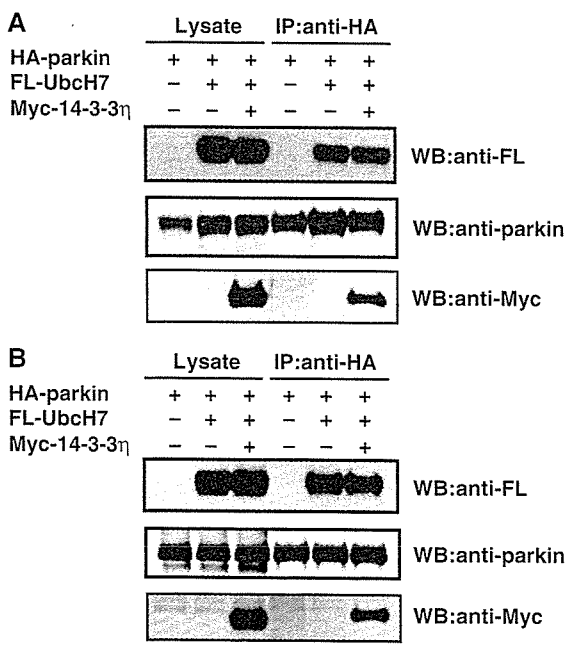

Figure 4 Effect of 14-3-3η on the recruitment of E2 (UbcH7 or Ubc7) to parkin. (**A**) HA-parkin (3 μg), FL-UbcH7 (3 μg), or Myc-14-3-3η (6 μg) plasmids were transfected for 48 h into HEK293 cells at the indicated combinations. After immunoprecipitation with anti-HA antibody, Western blotting was performed using antibodies against FL, Myc, and parkin. (**B**) The experiment was conducted as in (A), except that FL-Ubc7 was used instead of FL-UbcH7.

We also tested the interaction of Myc-14-3-3η with FL-α-SN, FL-α-SN(A30P), and FL-α-SN(A53T). Myc-14-3-3η interacted only with FL-α-SN, but not α-SN(A30P) nor α-SN(A53T) (Figure 5C, upper-top panel), suggesting that α-SN relieves parkin activity from binding to 14-3-3η. The 14-3-3η/α-SN interaction was not affected by parkin (Figure 5C, upper-top panel), and parkin was not associated with α-SN (Figure 5C, upper-second panel). Interestingly, FL-α-SN did not interact with Myc-14-3-3σ, β, and ζ in the same experiment (Figure 5C, lower panel). These results further strengthen the notion that α-SN specifically activates parkin through binding 14-3-3η.

We then investigated whether the interaction of 14-3-3η and parkin is direct or indirect by using purified recombinant His-parkin and GST-14-3-3η. GST or GST-14-3-3η was mixed with His-parkin, and pulled down by glutathione beads. His-parkin bound to GST-14-3-3η, but not GST (Figure 5D, left panel), indicating that parkin directly interacts with 14-3-3η. On the other hand, a similar *in vitro* binding assay showed that GST-14-3-3η did not interact with recombinant α-SN (Figure 5D, right panel), suggesting that certain modification(s) of α-SN may be required for the interaction of 14-3-3η.

Subsequently, we measured the binding affinities of parkin and α-SN for 14-3-3η by the surface plasmon resonance (SPR) method. As shown in Figure 5E, parkin bound 14-3-3η with a considerably strong affinity ($K_d = 4.2$ nM, upper), whereas the affinity of α-SN for 14-3-3η was much lower than that of parkin ($K_d = 1.1$ μM, lower). These results are consistent with those of the immunoprecipitation/Western analysis using recombinant proteins (Figure 5D).

Finally, we examined whether 14-3-3η bound to parkin can be released by α-SN. To test this, we first mixed the lysates coexpressing FL-parkin and Myc-14-3-3η of HEK293 cells with those expressing α-SN. Then the mixtures were incubated under three different conditions, as indicated in the upper panel of Figure 5F. Next, the lysates were immunoprecipitated with anti-FL antibody, and followed by Western blotting with anti-Myc and anti-parkin antibodies. As shown in Figure 5F (upper panel), the amount of 14-3-3η bound to parkin was significantly lower in all incubation conditions, when the cell lysates that simultaneously expressed both parkin and 14-3-3η were incubated with α-SN-expressing lysates. Incubation for 1 h at 37°C reduced the amount of 14-3-3η bound to parkin in proportion to the added amount of α-SN-expressing cell lysate (Figure 5F, lower panel). Intriguingly, the α-SN(A30P) and α-SN(A53T) mutants had no effect on the release of 14-3-3η, unlike wild-type (WT) α-SN (Figure 5F, lower panel). These observations strongly indicate that α-SN, but not α-SN(A30P) or α-SN(A53T), can capture and release 14-3-3η from the parkin–14-3-3η complex, which supports our notion that the negative regulation of parkin activity by 14-3-3η is relieved by α-SN (Figure 5A and B).

Parkin, 14-3-3η, and α-SN levels in the substantia nigra of PD

Finally, we analyzed the levels of parkin, 14-3-3η, and α-SN in the substantia nigra of the midbrain from patients with sporadic PD. Western blotting revealed no significant differences in parkin, 14-3-3η, and actin in the substantia nigra between control (patients without PD) and PD patients, whereas α-SN was significantly increased in the substantia nigra of PD patients (Figure 6A, upper panel). As parkin did not interact physically with α-SN in our immunoprecipitation analysis (Figure 5C; data not shown), we then examined the interactions of 14-3-3η with parkin or α-SN by measuring

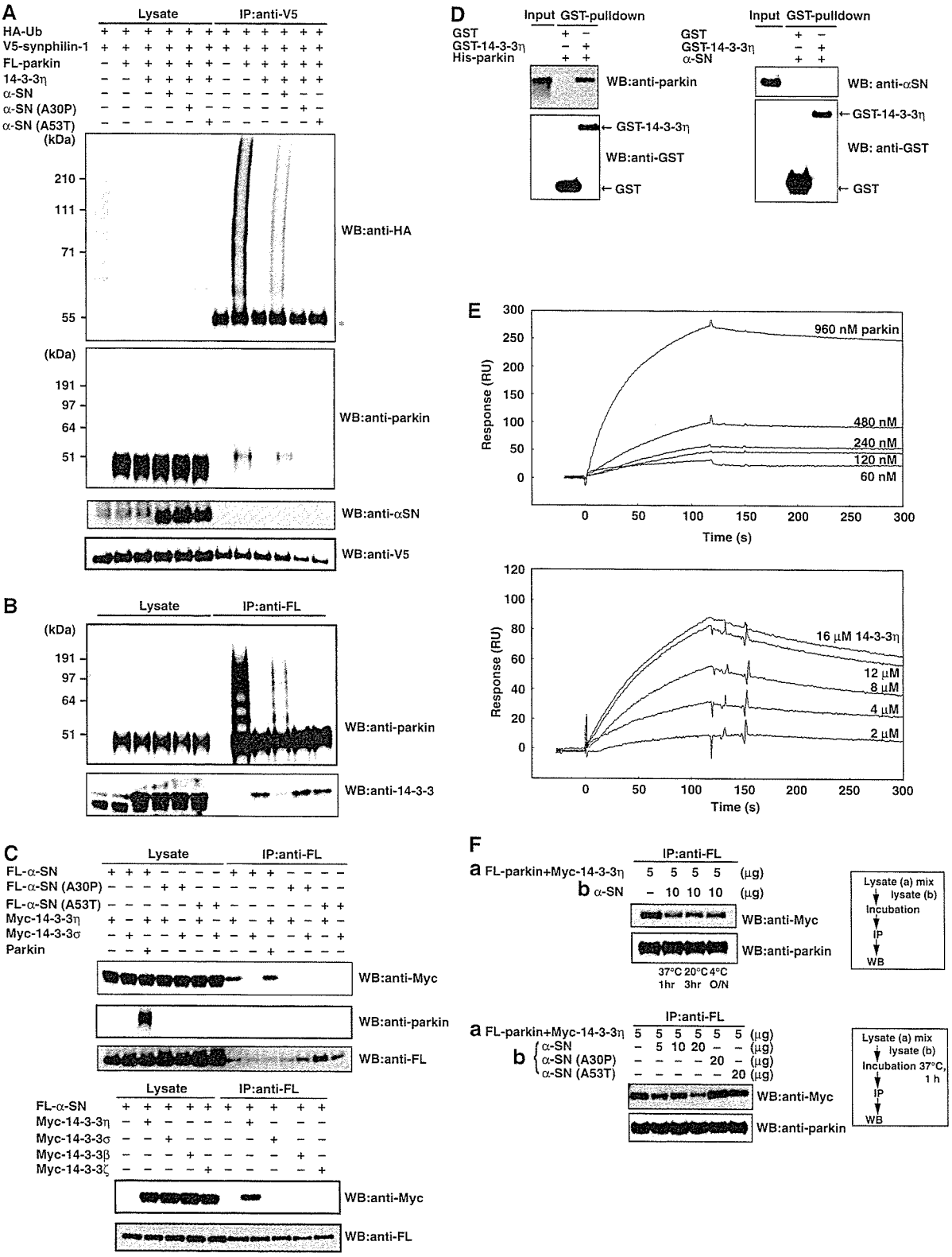

these proteins in the anti-14-3-3η immunoprecipitant. Whereas the levels of parkin associated with 14-3-3η from PD appeared to be decreased relative to the control, the levels of α-SN that interacted with 14-3-3η were clearly increased in patients with PD (Figure 6A, lower panel). Thus, it is suggested that the elevated levels of α-SN are associated with its interaction with 14-3-3η and the activity of parkin may be aberrantly regulated in the substantia nigra of sporadic PD.

Discussion

The major finding of the present study was the identification of 14-3-3η as a novel regulator of parkin. First, parkin was in a complex with 14-3-3η, but not β, γ, ε, or τ isoforms, in the mouse brain (Figure 1). 14-3-3η could bind primarily to the linker region of parkin, but not with the ARJP-causing missense mutant parkin (K161N), which has a mutation in the

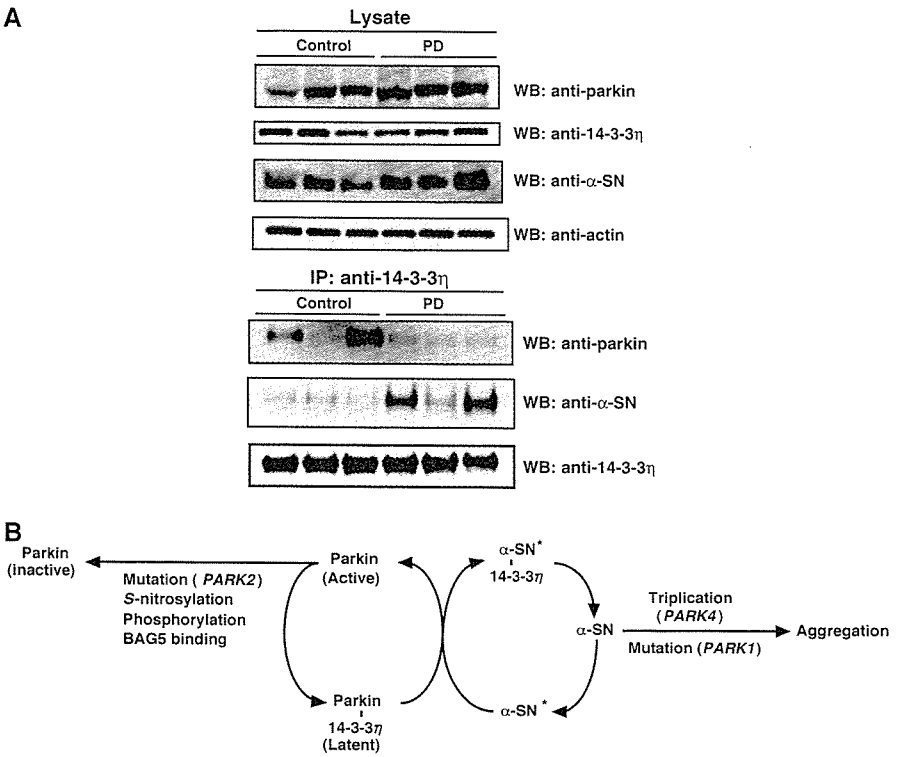

Figure 6 (**A**) Levels of parkin, 14-3-3η, and α-SN in the substantia nigra of PD. Brain of a representative patient with PD (upper panel). Samples (30 μg) of the crude extract of the brains (substantia nigra) of control (patients without PD) and PD patients were subjected to SDS–PAGE, following Western blotting against antibodies against parkin, 14-3-3η, α-SN, and actin. Physical interaction between 14-3-3η and parkin or α-SN (lower panel). After the same samples used in the upper panel were immunoprecipitated with anti-14-3-3η, Western blotting was carried out using antibodies against parkin, α-SN, and 14-3-3η. (**B**) A schematic diagram showing the pathways involved in the regulation of parkin activity by 14-3-3η and α-SN. α-SN, α-synuclein; α-SN*, modified form of α-SN. Note that whether parkin is phosphorylated to bind to 14-3-3η remains unknown at present. See text for details.

Figure 5 Effects of α-SN on 14-3-3η-induced suppression of parkin E3 activity and interaction between 14-3-3η and α-SN in HEK293 cells. (**A**) Ubiquitylation of synphilin-1. Transfection was conducted at various combinations, as in Figure 3C, except for cotransfection of 4 μg of α-SN, α-SN(A30P), and α-SN(A53T). After immunoprecipitation with anti-V5 antibody, Western blotting was carried out with antibodies against HA, parkin and α-SN, and V5. Asterisk denotes an IgG heavy chain. (**B**) Autoubiquitylation of parkin. Transfection was performed as in (A). After immunoprecipitation with anti-FL antibody, Western blotting was carried out with antibodies against parkin and 14-3-3. (**C**) Interaction of 14-3-3η and α-SN with or without parkin. Various expression vectors at the indicated combinations were transfected. Immunoprecipitation was conducted by anti-FL antibody and the resulting immunoprecipitates were used for Western blotting with antibodies against Myc, parkin, and FL. (**D**) Physical interaction between 14-3-3η and parkin (left panel) or α-SN (right panel) in recombinant proteins. After recombinant His-tagged parkin produced from baculovirus-infected HiFive insect cells (3 μg) or GST-α-SN expressed in *E. coli* whose GST moiety was removed by PreScission Protease digestion prior to use (3 μg) was incubated for 1 h at 32°C with 3 μg of GST or GST-tagged 14-3-3η expressed in *E. coli*, glutathione-Sepharose was added and the incubation vessels were slowly rotated for 3 h at 4°C. The washed Sepharose resin was eluted with 50 μl of 50 mM Tris–HCl (pH 8.0) buffer containing 10 mM reduced glutathione, and aliquots (15 μl) were analyzed by Western blotting with antibodies against parkin (left-top panel), α-SN (right-top panel), and GST (bottom panel). Input: 500 ng of parkin or α-SN. (**E**) SPR analyses of parkin and α-SN binding to 14-3-3η. Upper: subtracted sensorgrams of interaction between a subset of parkin concentrations and immobilized 14-3-3η. Lower: subtracted sensorgrams of interaction between a subset of 14-3-3η concentrations and immobilized α-SN. (**F**) Sequestration of 14-3-3η by α-SN from the parkin–14-3-3η complex. Various expression vectors were transfected as indicated. Upper panel: 5 μg of the lysate-(a) from cells co-expressing FL-parkin and Myc-14-3-3η were mixed with 10 μg of cellular lysate-(b) expressing α-SN. The mixtures were incubated under various conditions; that is, 37°C for 1 h, 20°C for 3 h, or overnight at 4°C (O/N), then immunoprecipitation by anti-FL antibody was conducted, followed by Western blotting with antibodies against Myc (14-3-3η) and parkin. Lower panel: the experiments were conducted as for the top panel, except that incubation was carried out at 37°C for 1 h using α-SN-, α-SN(A30P)-, or α-SN (A53T)-expressing lysates as indicated. The experimental protocol is shown in the flow charts on the right.

linker region (Figure 2). Second, the binding of 14-3-3η to parkin was associated with suppression of the ubiquitin-ligase activity, suggesting that certain parkin bound to 14-3-3η is present at a latent status in the brain (Figure 3). Third, overexpression of α-SN abrogated the 14-3-3η-induced suppression of parkin activity, indicating that α-SN relieves the negative regulation of parkin by 14-3-3η (Figure 5A and B). Intriguingly, PD-causing A30P and A53T mutations of α-SN could not bind 14-3-3η and failed to activate parkin. These results indicate that 14-3-3η is a regulator that functionally links parkin and α-SN, as illustrated in Figure 6B.

It is of particular note that we report unusual isoform specificity for 14-3-3η to interact with parkin among all 14-3-3 species examined. However, the possibility that the other species are also involved in the interaction by forming a heterodimer with 14-3-3η cannot be excluded *in vivo*, because 14-3-3 bands immunoprecipitated by anti-parkin antibody from the brain extracts showed doublet with one weak signal for Western blotting (Figure 1A). Nevertheless, herein we address that recombinant parkin could directly bind to 14-3-3η (Figure 5D, left panel), with considerably high affinity (K_d = approximately 4 nM) (Figure 5E) and that the 14-3-3η homodimer is a negative factor for autoubiquitylating activity of parkin *in vitro* (Figure 3A).

It is known that the 14-3-3 family proteins interact with the majority, but not all, proteins after their phosphorylation (Aitken *et al*, 2002; Bridges and Moorhead, 2004; Mackintosh, 2004). Indeed, parkin contains the RKDSPP sequence in the linker region that resembles the typical binding motifs with a potential phosphorylation residue for 14-3-3 proteins (Yaffe *et al*, 1997; Mackintosh, 2004). It is also known that parkin has several possible phosphorylation sites, and recent studies showed that parkin is phosphorylated *in vitro* (Yamamoto *et al*, 2004), although there is no direct evidence demonstrating phosphorylation of parkin *in vivo* to date. However, it remains elusive whether or not phosphorylation of parkin is responsible for its specific binding to 14-3-3η, because known potential phosphorylation motifs are capable of associating with many 14-3-3 species in general. The specificities of 14-3-3: client–protein interactions do not result from different specificities for the phosphopeptide-binding motifs, but probably arises from contacts made on the variable surface of 14-3-3 outside the binding cleft, as discussed previously by Yaffe *et al* (1997). In this regard, some reports showed functional specificities of 14-3-3 isoforms (Aitken, 2002; Aitken *et al*, 2002; Roberts and de Bruxelles, 2002), and indeed several enzymes retain several nonphosphorylated binding motifs for 14-3-3s (Hallberg, 2002; Sribar *et al*, 2003), though parkin lacks such 14-3-3-interacting sequences. Thus, parkin, in particular its linker region, may have a new binding motif(s) for 14-3-3η, but the interacting motif(s) remains to be identified. If 14-3-3η binds to parkin through two sites as a dimmer, it is plausible that the phosphorylation of parkin is involved in their interactions at least in part.

With regard to the mechanistic action of 14-3-3η, it may suppress parkin activity by preventing access of the substrate, because the binding of synphilin-1 (used here as a model substrate to parkin) was inhibited by 14-3-3η (Figure 3C). Accumulating evidence suggests that parkin can bind various targets by the UBL domain or the RING box, in particular the RING 1 domain (Dawson and Dawson, 2003). Accordingly, 14-3-3η may have function(s) other than suppressing the access of the substrate to parkin. Indeed, 14-3-3η strongly inhibits substrate-independent self-ubiquitylation of parkin, indicating blockage of the intrinsic E3 activity. It was also anticipated that 14-3-3η hinders the recruitment of E2 to parkin. However, this was not the case, because 14-3-3η had no effect on the binding of UbcH7 and Ubc7 to parkin (Figure 4). Thus, while the mechanism of 14-3-3η-induced suppression of parkin activity remains to be identified, it is possible that it involves preventing the positioning of the ubiquitin-charged E2 toward the target Lys residue by steric hindrance due to the association of 14-3-3η to parkin.

It is worth noting that parkin does not interact with α-SN directly, because we could not demonstrate the physical binding of parkin to α-SN *in vivo* and *in vitro* (data not shown; see also Dawson and Dawson, 2003). Nevertheless, we found that the negative regulation of parkin by 14-3-3η was relieved by α-SN, which could bind tightly to 14-3-3η *in vivo* (Figure 5A–C). In this regard, it is of note that the amounts of 14-3-3η bound to parkin were decreased when the lysates of cells coexpressing parkin and 14-3-3η were incubated with those expressing WT α-SN, but not PD-related α-SN(A30P) or α-SN(A53T) mutants *in vitro* (Figure 5F). These results clearly indicate that 14-3-3η bound to parkin is sequestered by α-SN, but not competition by α-SN toward the binding of 14-3-3η to parkin. Unlike the association between parkin and 14-3-3η, there is little or no interaction between α-SN and 14-3-3η *in vitro*, as recombinant α-SN did not bind to 14-3-3η (Figure 5D, right panel, and E). Thus, it is plausible that certain modification(s) of α-SN is required for its association to 14-3-3η in mammalian cells (see our model in Figure 6B). Judging from the characteristic properties of 14-3-3 family proteins capable of binding many phosphorylated proteins (Yaffe *et al*, 1997), certain phosphorylation(s) of α-SN seems quite possible for the interaction with 14-3-3η. Indeed, there are several reports regarding phosphorylation of α-SN (Fujiwara *et al*, 2002; Hirai *et al*, 2004). Although previous studies clearly demonstrated that α-SN deposited in synucleinopathy brains is extensively phosphorylated at Ser-129 (Fujiwara *et al*, 2002; Hirai *et al*, 2004), this is probably not the case in our study, because the chemically synthesized peptide phosphorylated at Ser-129 of α-SN did not bind to the 14-3-3η (our unpublished results). However, the possibility that α-SN is phosphorylated at other site(s) cannot be exclusively ruled out. Alternatively, one cannot exclude a possible, though yet unknown, modification(s) of α-SN other than phosphorylation as a mechanism responsible for the increased affinity toward 14-3-3η. In this regard, α-SN is structurally related to 14-3-3 family proteins (Ostrerova *et al*, 1999), but it is unknown whether the homologous region is involved in the physical interaction with α-SN. Further studies are required to clarify the mode of α-SN modification.

In the present study, we found reciprocal regulation of parkin activity by α-SN and 14-3-3η, whose tripartite control could enhance our understanding of the pathogenesis of PD. As illustrated in Figure 6B, to date there are several reports on the post-translational modification of parkin. Recent findings indicate that the ubiquitin E3 ligase activity of parkin is modified by nitric oxide (NO). Namely, parkin is *S*-nitrosylated in PD patients and an *in vivo* mouse model of PD, and *S*-nitrosylation shows inhibition of the E3 activity of

parkin (Chung *et al*, 2004; Kahle and Haass, 2004; Yao *et al*, 2004), which could contribute to the degenerative process in PD by impairing the ubiquitylation of parkin substrates. Moreover, Kalia *et al* (2004) showed that the bcl-2-associated athanogene 5 (BAG5) enhanced the death of dopaminergic neurons in an *in vivo* model of PD by inhibiting the E3 ligase activity of parkin. In addition, recent studies reported that phosphorylation of parkin causes a small but significant reduction of parkin auto-ubiquitylating activity (Yamamoto *et al*, 2004). More recently, it was reported that Nrdp1/FLRF RING-finger E3 ligase binds and ubiquitylates parkin, resulting in reduction of parkin activity, implying its involvement in the pathogenesis of PD (Zhong *et al*, 2005). Considered together, these results indicate that the apparent loss of parkin E3 ubiquitin ligase activity associated with the pathogenesis of PD (see the model displayed in Figure 6B) is in agreement with the ARJP-linked mutations that lead to loss of function of parkin, and that the functional loss of parkin activity is linked to the death of dopaminergic neurons. In addition, we reported herein the imbalance of tripartite interactions among parkin, 14-3-3η, and α-SN levels in the substantia nigra of sporadic PD, but it is still not clear how these alterations influence parkin activity in neural cells. Thus, parkin is an E3 ubiquitin ligase involved in the ubiquitylation of proteins, irrespective of its involvement of K48- or K63-linked ubiquitylation (Doss-Pepe *et al*, 2005; Lim *et al*, 2005), that are important in the survival of dopaminergic neurons in PD.

In the present study, we found that parkin E3 activity is regulated positively and negatively by α-SN and 14-3-3η, respectively, suggesting that derangements of this regulation may be responsible for ARJP. For instance, the activated parkin free from 14-3-3η may be labile, and thus sensitive to other stresses, such as *S*-nitrosylation, and inactivated secondarily in PD. This situation resembles the effect of *S*-nitrosylation, in which nitrosative stress leads to *S*-nitrosylation of WT parkin, which leads initially to a marked increase followed by a decrease in the E3 ligase–ubiquitin–proteasome degradative pathway (Yao *et al*, 2004). The initial increase in the activity of parkin's E3 ubiquitin ligase leads to autoubiquitylation of parkin and subsequent inhibition of its activity, which would impair ubiquitylation and clearance of parkin substrates. In turn, 14-3-3η may protect against impairment of parkin induced by various environmental stresses, including *S*-nitrosylation. It is also noteworthy that, although 14-3-3η acts as a negative regulator of parkin, it may play a positive role in maintaining a large pool of parkin by preventing its self-ubiquitylation in the brain. Finally, we assume that gradual reduction of parkin activity may be associated with the development of ARJP as well as sporadic PD.

Current evidence suggests that α-SN increases in response to various stresses (Sherer *et al*, 2002; Gomez-Santos *et al*, 2003). This finding is compatible with the results of recent studies that dopamine-dependent neurotoxicity (Tabrizi *et al*, 2000; Zhou *et al*, 2000; Junn and Mouradian, 2002) is mediated by the formation of protein complexes that contain α-SN and 14-3-3, which are selectively increased in the substantia nigra in PD (Xu *et al*, 2002). Further studies are needed to determine the levels of parkin, 14-3-3η, α-SN, and parkin and α-SN-14-3-3η complexes in the substantia nigra of the midbrain of patients with sporadic PD.

Here we suggest that α-SN and parkin function through the same pathway. Indeed, both proteins, if not all, are associated with presynaptic vesicles (Dawson and Dawson, 2003). So far, however, the physiological role of α-SN is largely unknown, though various roles including its involvement in synaptic plasticity have been suggested (Liu *et al*, 2004). We here provided the first evidence that α-SN acts as a positive regulator of parkin E3 activity. It is worth noting that disease-causing mutations of α-SN(A30P) and α-SN(A53T) could not activate the latent parkin–14-3-3η complex, and thus, these mutations may accelerate the development of PD by failing to activate parkin. Our results identified a functional link between these two familial PD-gene products, thus highlighting the existence of a novel regulatory mechanism that could help us further understand the pathogenesis of ARJP as well as sporadic PD. However, it must be stressed here that α-SN is the causative gene product of familial PD. It is noteworthy that α-SN is an aggregation-prone protein due to its natively unfolded protein nature. It is of note that the locus of *PARK4* is triplication of the *α-SN* gene (*PARK1*) (Singleton *et al*, 2003), indicating that overexpression of α-SN itself is toxic and induces dopaminergic neuronal death. Indeed, α-SN tends to self-aggregate, and this tendency, which is augmented in the α-SN(A30P) and α-SN(A53T) mutants (Conway *et al*, 2000) (see our model in Figure 6B), causes autosomal dominant PD (Narhi *et al*, 1999). Both WT and mutant α-SN form amyloid fibrils akin to those seen in LBs, as well as nonfibrillary oligomers termed protofibrils (Dawson and Dawson, 2003; Bossy-Wetzel *et al*, 2004). However, whether aggregation and fibrillary formation of α-SN- and PD-linked mutants play a role in neuronal dysfunction and death of neurons in PD are a matter of fierce debate. At this point of view, we emphasize that the feature of α-SN as an aggregation-prone protein is probably not linked directly to its role as a potent activator of parkin E3 in the pathogenesis of PD. Even if these two unique properties of α-SN account for the development of PD independently or synergistically, however, it is clear that their mechanistic actions differ as illustrated in Figure 6B.

Materials and methods

Immunological analysis

For immunoprecipitation analysis of endogenous proteins in the brains of adult mouse and human, these brains were homogenized in three volumes of ice-cold lysis buffer (20 mM HEPES (pH 7.9) buffer containing 0.2% NP-40, 1 mM dithiothreitol (DTT) and protease inhibitor cocktail (Sigma, Chemical Co., St Louis, MO)). The tissue homogenate was centrifuged at 20 000 *g* at 4°C for 20 min. The supernatant (2 mg protein) was used for immunoprecipitation with one of the following antibodies: anti-polyclonal parkin (Cell Signaling Technology, Beverly, MA) and anti-14-3-3η antibodies (Immuno-Biological Lab. Co., Gunma) or control IgG (700 ng). The resulting immunoprecipitates were resolved in 30 μl of the sodium dodecyl sulfate–polyacrylamide gel electrophoresis (SDS–PAGE) sample buffer, and one-third of the samples (10 μl) were subjected to SDS–PAGE, followed by Western blotting with anti-14-3-3 (Santa Cruz Biotechnology, Santa Cruz, CA), anti-14-3-3β, 14-3-3γ, 14-3-3ε, 14-3-3η, and 14-3-3τ (Immuno-Biological Lab. Co., Ltd, Japan) and anti-monoclonal parkin (1A1) antibodies (Shimura *et al*, 1999). In all, 10 μg of the supernatant (lysate) was used as input (1.5%).

For immunoprecipitation analysis of the cell culture system, HEK293 cells were transfected with the respective plasmids. After 48 h, the cells were washed with ice-cold PBS (in mM, 10 Na_2PO_4, 2 KH_2PO_4, 137 NaCl, and 2.7 KCl), pH 7.4, and harvested in the lysis buffer (600 μl). The lysate was then rotated at 4°C for 1 h, followed by centrifugation at 20 000 *g* for 10 min. The supernatant (200 μl) was then combined with 50 μl protein G-Sepharose (Amersham Life

Science, Buckinghamshire, UK), pre-incubated with anti-Myc (Santa Cruz Biotechnology, Santa Cruz), V5 (Invitrogen), and HA (Santa Cruz Biotechnology) antibodies or anti-FL antibody beads (Sigma) for 3 h. The protein G-Sepharose or FL-beads were precipitated and the pellets were extensively washed using the lysis buffer containing 500 mM NaCl. The precipitates were used for Western blot analysis using anti-parkin, Myc, FL, HA, V5, 14-3-3, and α-SN (BD Transduction Lab.) antibodies, as mentioned above. A volume of 5 μl of the supernatant was used as input (7.5%).

In vitro autoubiquitylation assay

Recombinant GST-14-3-3η was produced in *Escherichia coli*. Untagged 14-3-3η was produced from GST-14-3-3η by digestion with PreScission Protease (Amersham Bioscience). Recombinant His-parkin and E1 were produced from baculovirus-infected HiFive insect cells. Reactions were performed for 3 h at 37°C in 50 μl of assay mixture containing 40 mM Tris–HCl buffer (pH 7.5), 5 mM $MgCl_2$, 2 mM ATP, 2 mM DTT, 15 μg ubiquitin (Sigma), 200 ng of E1, and 600 ng of E2 (UbcH7) (Affiniti-Research, Exeter, Devon, UK) in the presence or absence of GST-14-3-3η or 14-3-3η. After incubation, the reaction was terminated by the addition of the sample buffer for SDS–PAGE (17 μl), and aliquots (15 μl) were subjected to SDS–PAGE followed by Western blotting with anti-parkin antibody.

In vivo ubiquitylation assay

HEK293 cells were transfected for 48 h with pcDNA3.1 expression plasmids, in which FL-tagged parkin or FL-parkin mutants, α-SN or α-SN mutants, 14-3-3η, V5-synphilin-1, and HA-ubiquitin cDNAs were ligated. MG132 (50 μM) was added for 20 min, prior to harvesting of the cells. Then, the cells were washed with cold PBS and lysed by 50 mM Tris–HCl buffer (pH 8.0), containing 150 mM NaCl, 1% Nonidet-P40, 1% deoxycolate, 0.1% SDS, 5 mM ethylenediaminetetraacetic acid, and protease inhibitor cocktail. Preparation of the cell lysate, immunoprecipitation, and Western blot analyses were essentially the same for the immunological analysis as described above. In all experiments, the cell lysates (10 μg, 7.5% input) were used for Western blotting as controls to check the expression levels.

For the method sections of 'Cell culture and transfection', 'Plasmids', and 'Surface plasmon resonance (SPR) analysis', see Supplementary data.

Supplementary data

Supplementary data are available at *The EMBO Journal* Online.

Acknowledgements

We thank Y Goto for providing the 14-3-3σ, β, and ζ expression plasmids, and T Ichimura for the valuable discussion. This work was supported in part by Grants-in-Aid from the Ministry of Education, Culture, Sports, Science and Technology of Japan.

References

Aitken A (2002) Functional specificity in 14-3-3 isoform interactions through dimer formation and phosphorylation. Chromosome location of mammalian isoforms and variants. *Plant Mol Biol* **50:** 993–1010

Aitken A, Baxter H, Dubois T, Clokie S, Mackie S, Mitchell K, Peden A, Zemlickova E (2002) Specificity of 14-3-3 isoform dimer interactions and phosphorylation. *Biochem Soc Trans* **30:** 351–360

Baxter HC, Liu WG, Forster JL, Aitken A, Fraser JR (2002) Immunolocalisation of 14-3-3 isoforms in normal and scrapie-infected murine brain. *Neuroscience* **109:** 5–14

Berg D, Holzmann C, Riess O (2003) 14-3-3 proteins in the nervous system. *Nat Rev Neurosci* **4:** 752–762

Bossy-Wetzel E, Schwarzenbacher R, Lipton SA (2004) Molecular pathways to neurodegeneration. *Nat Med* **10** (Suppl S2): S2–S9

Bridges D, Moorhead GB (2004) 14-3-3 proteins: a number of functions for a numbered protein. *Sci STKE* **2004:** re10

Chung KK, Thomas B, Li X, Pletnikova O, Troncoso JC, Marsh L, Dawson VL, Dawson TM (2004) *S*-nitrosylation of parkin regulates ubiquitination and compromises parkin's protective function. *Science* **304:** 1328–1331

Chung KK, Zhang Y, Lim KL, Tanaka Y, Huang H, Gao J, Ross CA, Dawson VL, Dawson TM (2001) Parkin ubiquitinates the α-synuclein-interacting protein, synphilin-1: implications for Lewy-body formation in Parkinson disease. *Nat Med* **7:** 1144–1150

Conway KA, Lee SJ, Rochet JC, Ding TT, Williamson RE, Lansbury Jr PT (2000) Acceleration of oligomerization, not fibrillization, is a shared property of both α-synuclein mutations linked to early-onset Parkinson's disease: implications for pathogenesis and therapy. *Proc Natl Acad Sci USA* **97:** 571–576

Dawson TM, Dawson VL (2003) Molecular pathways of neurodegeneration in Parkinson's disease. *Science* **302:** 819–822

Doss-Pepe EW, Chen L, Madura K (2005) α-Synuclein and parkin contribute to the assembly of ubiquitin lysine 63-linked multiubiquitin chains. *J Biol Chem* **280:** 16619–16624

Forno LS (1996) Neuropathology of Parkinson's disease. *J Neuropathol Exp Neurol* **55:** 259–272

Fujiwara H, Hasegawa M, Dohmae N, Kawashima A, Masliah E, Goldberg MS, Shen J, Takio K, Iwatsubo T (2002) α-Synuclein is phosphorylated in synucleinopathy lesions. *Nat Cell Biol* **4:** 160–164

Gomez-Santos C, Ferrer I, Santidrian AF, Barrachina M, Gil J, Ambrosio S (2003) Dopamine induces autophagic cell death and α-synuclein increase in human neuroblastoma SH-SY5Y cells. *J Neurosci Res* **73:** 341–350

Hallberg B (2002) Exoenzyme S binds its cofactor 14-3-3 through a non-phosphorylated motif. *Biochem Soc Trans* **30:** 401–405

Hirai Y, Fujita SC, Iwatsubo T, Hasegawa M (2004) Phosphorylated α-synuclein in normal mouse brain. *FEBS Lett* **572:** 227–232

Imai Y, Soda M, Inoue H, Hattori N, Mizuno Y, Takahashi R (2001) An unfolded putative transmembrane polypeptide, which can lead to endoplasmic reticulum stress, is a substrate of Parkin. *Cell* **105:** 891–902

Junn E, Mouradian MM (2002) Human α-synuclein over-expression increases intracellular reactive oxygen species levels and susceptibility to dopamine. *Neurosci Lett* **320:** 146–150

Kahle PJ, Haass C (2004) How does parkin ligate ubiquitin to Parkinson's disease? *EMBO Rep* **5:** 681–685

Kalia SK, Lee S, Smith PD, Liu L, Crocker SJ, Thorarinsdottir TE, Glover JR, Fon EA, Park DS, Lozano AM (2004) BAG5 inhibits parkin and enhances dopaminergic neuron degeneration. *Neuron* **44:** 931–945

Kawakami T, Chiba T, Suzuki T, Iwai K, Yamanaka K, Minato N, Suzuki H, Shimbara N, Hidaka Y, Osaka F, Omata M, Tanaka K (2001) NEDD8 recruits E2-ubiquitin to SCF E3 ligase. *EMBO J* **20:** 4003–4012

Kawamoto Y, Akiguchi I, Nakamura S, Honjyo Y, Shibasaki H, Budka H (2002) 14-3-3 proteins in Lewy bodies in Parkinson disease and diffuse Lewy body disease brains. *J Neuropathol Exp Neurol* **61:** 245–253

Kruger R, Kuhn W, Muller T, Woitalla D, Graeber M, Kosel S, Przuntek H, Epplen JT, Schols L, Riess O (1998) A30P mutation in the gene encoding α-synuclein in Parkinson's disease. *Nat Genet* **18:** 106–108

Lim KL, Chew KC, Tan JM, Wang C, Chung KK, Zhang Y, Tanaka Y, Smith W, Engelender S, Ross CA, Dawson VL, Dawson TM (2005) Parkin mediates nonclassical, proteasomal-independent ubiquitination of synphilin-1: implications for Lewy body formation. *J Neurosci* **25:** 2002–2009

Liu S, Ninan I, Antonova I, Battaglia F, Trinchese F, Narasanna A, Kolodilov N, Dauer W, Hawkins RD, Arancio O (2004) Synuclein produces a long-lasting increase in neurotransmitter release. *EMBO J* **23:** 4506–4516

Mackintosh C (2004) Dynamic interactions between 14-3-3 proteins and phosphoproteins regulate diverse cellular processes. *Biochem J* **381:** 329–342

Martin H, Rostas J, Patel Y, Aitken A (1994) Subcellular localisation of 14-3-3 isoforms in rat brain using specific antibodies. *J Neurochem* **63:** 2259–2265

McNaught KS, Olanow CW (2003) Proteolytic stress: a unifying concept for the etiopathogenesis of Parkinson's disease. *Ann Neurol* **53** (Suppl 3): S73–S84

Narhi L, Wood SJ, Steavenson S, Jiang Y, Wu GM, Anafi D, Kaufman SA, Martin F, Sitney K, Denis P, Louis JC, Wypych J, Biere AL, Citron M. (1999) Both familial Parkinson's disease mutations accelerate α-synuclein aggregation. *J Biol Chem* **274**: 9843–9846

Ostrerova N, Petrucelli L, Farrer M, Mehta N, Choi P, Hardy J, Wolozin B (1999) α-Synuclein shares physical and functional homology with 14-3-3 proteins. *J Neurosci* **19**: 5782–5791

Polymeropoulos MH, Lavedan C, Leroy E, Ide SE, Dehejia A, Dutra A, Pike B, Root H, Rubenstein J, Boyer R, Stenroos ES, Chandrasekharappa S, Athanassiadou A, Papapetropoulos T, Johnson WG, Lazzarini AM, Duvoisin RC, Di Iorio G, Golbe LI, Nussbaum RL (1997) Mutation in the α-synuclein gene identified in families with Parkinson's disease. *Science* **276**: 2045–2047

Roberts MR, de Bruxelles GL (2002) Plant 14-3-3 protein families: evidence for isoform-specific functions? *Biochem Soc Trans* **30**: 373–378

Sherer TB, Betarbet R, Stout AK, Lund S, Baptista M, Panov AV, Cookson MR, Greenamyre JT (2002) An *in vitro* model of Parkinson's disease: linking mitochondrial impairment to altered α-synuclein metabolism and oxidative damage. *J Neurosci* **22**: 7006–7015

Shimura H, Hattori N, Kubo S, Mizuno Y, Asakawa S, Minoshima S, Shimizu N, Iwai K, Chiba T, Tanaka K, Suzuki T (2000) Familial Parkinson disease gene product, parkin, is a ubiquitin-protein ligase. *Nat Genet* **25**: 302–305

Shimura H, Hattori N, Kubo S, Yoshikawa M, Kitada T, Matsumine H, Asakawa S, Minoshima S, Yamamura Y, Shimizu N, Mizuno Y (1999) Immunohistochemical and subcellular localization of Parkin protein: absence of protein in autosomal recessive juvenile parkinsonism patients. *Ann Neurol* **45**: 668–672

Singleton AB, Farrer M, Johnson J, Singleton A, Hague S, Kachergus J, Hulihan M, Peuralinna T, Dutra A, Nussbaum R, Lincoln S, Crawley A, Hanson M, Maraganore D, Adler C, Cookson MR, Muenter M, Baptista M, Miller D, Blancato J, Hardy J, Gwinn-Hardy K (2003) α-Synuclein locus triplication causes Parkinson's disease. *Science* **302**: 841

Sribar J, Sherman NE, Prijatelj P, Faure G, Gubensek F, Fox JW, Aitken A, Pungercar J, Krizaj I (2003) The neurotoxic phospholipase A2 associates, through a non-phosphorylated binding motif, with 14-3-3 protein γ and ε isoforms. *Biochem Biophys Res Commun* **302**: 691–696

Tabrizi SJ, Orth M, Wilkinson JM, Taanman JW, Warner TT, Cooper JM, Schapira AH (2000) Expression of mutant α-synuclein causes increased susceptibility to dopamine toxicity. *Hum Mol Genet* **9**: 2683–2689

Ubl A, Berg D, Holzmann C, Kruger R, Berger K, Arzberger T, Bornemann A, Riess O (2002) 14-3-3 protein is a component of Lewy bodies in Parkinson's disease-mutation analysis and association studies of 14-3-3η. *Brain Res Mol Brain Res* **108**: 33–39

Vila M, Przedborski S (2004) Genetic clues to the pathogenesis of Parkinson's disease. *Nat Med* **10** (Suppl): S58–S62

Xu J, Kao SY, Lee FJ, Song W, Jin LW, Yankner BA (2002) Dopamine-dependent neurotoxicity of α-synuclein: a mechanism for selective neurodegeneration in Parkinson disease. *Nat Med* **8**: 600–606

Yaffe MB, Rittinger K, Volinia S, Caron PR, Aitken A, Leffers H, Gamblin SJ, Smerdon SJ, Cantley LC (1997) The structural basis for 14-3-3:phosphopeptide binding specificity. *Cell* **91**: 961–971

Yamamoto A, Friedlein A, Imai Y, Takahashi R, Kahle PJ, Haass C (2004) Parkin phosphorylation and modulation of its E3 ubiquitin ligase activity. *J Biol Chem* **280**: 3390–3399

Yao D, Gu Z, Nakamura T, Shi ZQ, Ma Y, Gaston B, Palmer LA, Rockenstein EM, Zhang Z, Masliah E, Uehara T, Lipton SA (2004) Nitrosative stress linked to sporadic Parkinson's disease: S-nitrosylation of parkin regulates its E3 ubiquitin ligase activity. *Proc Natl Acad Sci USA* **101**: 10810–10814

Zhong L, Tan Y, Zhou A, Yu Q, Zhou J (2005) RING finger ubiquitin-protein isopeptide ligase Nrdp1/FLRF regulates parkin stability and activity. *J Biol Chem* **280**: 9425–9430

Zhou W, Hurlbert MS, Schaack J, Prasad KN, Freed CR (2000) Overexpression of human α-synuclein causes dopamine neuron death in rat primary culture and immortalized mesencephalon-derived cells. *Brain Res* **866**: 33–43

THE JOURNAL OF BIOLOGICAL CHEMISTRY VOL. 281, NO. 6, pp. 3204–3209, February 10, 2006

Diverse Effects of Pathogenic Mutations of Parkin That Catalyze Multiple Monoubiquitylation *in Vitro*[*] [S]

Received for publication, September 21, 2005, and in revised form, November 29, 2005 Published, JBC Papers in Press, December 8, 2005, DOI 10.1074/jbc.M510393200

Noriyuki Matsuda[‡], Toshiaki Kitami[§], Toshiaki Suzuki[‡], Yoshikuni Mizuno[§], Nobutaka Hattori[§], and Keiji Tanaka[‡1]

From the [‡]Laboratory of Frontier Science, Tokyo Metropolitan Institute of Medical Science, Bunkyo-ku, Tokyo 113-8613 and the [§]Department of Neurology, Juntendo University School of Medicine, 2-1-1 Hongo, Bunkyo-ku, Tokyo 113-0033, Japan

Mutational dysfunction of *PARKIN* gene, which encodes a double RING finger protein and has ubiquitin ligase E3 activity, is the major cause of autosomal recessive juvenile Parkinsonism. Although many studies explored the functions of Parkin, its biochemical character is poorly understood. To address this issue, we established an E3 assay system using maltose-binding protein-fused Parkin purified from *Escherichia coli*. Using this recombinant Parkin, we found that not the front but the rear RING finger motif is responsible for the E3 activity of Parkin, and it catalyzes multiple monoubiquitylation. Intriguingly, for autosomal recessive juvenile Parkinsonism-causing mutations of Parkin, whereas there was loss of E3 activity in the rear RING domain, other pathogenic mutants still exhibited E3 activity equivalent to that of the wild-type Parkin. The evidence presented allows us to reconsider the function of Parkin-catalyzed ubiquitylation and to conclude that autosomal recessive juvenile Parkinsonism is not solely attributable to catalytic impairment of the E3 activity of Parkin.

Recessive mutations in the human *PARKIN* gene are the most frequent cause of autosomal recessive juvenile parkinsonism, the common form of familial Parkinson disease (PD).[2] It has been shown that almost 50% of patients with familial autosomal recessive juvenile parkinsonism carry a series of exon rearrangements or point mutations in *PARKIN*. Moreover, recent findings of the haploinsufficiency of *parkin* and *S*-nitrosylation also imply its association in sporadic PD (1). The causal gene *PARKIN* encodes a double RING finger protein with ubiquitin ligase (E3) activity (2–5) and interestingly, missense mutations in the double RING finger motif resulted in an earlier onset of the disease than mutations in other function-unknown regions (6). To date, numerous biochemical studies have been performed to understand how mutations in Parkin lead to its dysfunction and to pathogenic outcome. However, because the biochemical characterization of E3 activity of Parkin has been difficult, it is still controversial whether the disease-relevant Parkin mutants lose their E3 activity or not. For example, one group of investigators implied that Parkin harboring K161N mutation loses its E3 activity (7), whereas another group suggested the same mutation dose not impair E3 activity (8). In the case of other PD mutations, the situation is even more complex (see supplemental Table 1). Thus, the mode of Parkin-catalyzed ubiquitylation remains poorly understood to date.

Little is known about the reconstituted ubiquitylating experiment using recombinant Parkin. Almost all of the biochemical analyses reported so far have been performed using *in vitro* translated Parkin or immunoprecipitated Parkin. However, it is difficult to avoid trace contaminants of other proteins that could physically interact with Parkin. Indeed it has been reported that Parkin interacts with other E3s such as CHIP (9) and Nrdp1/FLRF (10), and thus the results of experiments using immunoprecipitated or *in vitro* translated Parkin require careful interpretation. To study the E3 activity of intrinsic Parkin, a biochemical approach using bacterially expressed recombinant Parkin that is free from other contaminating E3 enzyme(s) is obviously required. We thus attempted to reconstitute a sensitive E3 assay system using Parkin purified from *Escherichia coli*.

EXPERIMENTAL PROCEDURES

Purification of Recombinant Proteins—To express Parkin in *E. coli*, it was important to use a modified *E. coli* strain BL21(DE3) codon-plus (RIL) strain (Stratagene, La Jolla, CA), because Parkin possesses many rare codons for *E. coli* that might cause low expression and/or amino acid misincorporation. For example, Parkin contains eight AGA codons that lead to mistranslation of lysine for arginine in *E. coli* (11). pMAL-p2T, in which the thrombin recognition site was inserted into pMALp2 (New England BioLabs, Beverly, MA), was prepared to purify maltose-binding protein (MBP)-LVPRGS-Parkin. Parkin cDNAs of wild type and various mutants/deletions were subcloned into BamHI site of pMAL-p2 and pMAL-p2T. All mutants/deletions were generated by PCR-mediated site-directed mutagenesis (details of the plasmid construction processes can be provided upon request). All recombinant fusion proteins were purified from bacterial lysate applying the method advocated by the supplier (New England BioLabs) using a column buffer containing 20 mM Tris-HCl, pH 7.5, 200 mM NaCl, 1 mM dithiothreitol, and 100 μM $ZnSO_4$. The eluted fraction containing 10 mM maltose was not dialyzed because Parkin tends to lose its E3 activity during dialysis. Instead, it was subjected to the ubiquitylation assay directly. We attempted to purify sole IBR-RING2 region of Parkin also by splitting MBP-IBR-RING2 (see "Results"). Specifically, we added E2, various detergents and stabilizers during the cleavage process expecting that they solubilize and/or stabilize free IBR-RING2 in solution. Even in all the above experimental conditions, however, we could not obtain soluble-free IBR-RING2 (data not shown). Six histidine-tagged proteins such as Uev1/Ubc13 were purified by the conventional method and dialyzed by a buffer containing 20 mM Tris-HCl, pH 8.0, 200 mM NaCl and 1 mM dithiothreitol. Glycerol of 6% was added as a stabilizer for preservation of recombinant MBP-Parkin and E2 proteins at −80 °C.

In Vitro Ubiquitylation Assay—The *in vitro* ubiquitylation assay was performed as described previously (12–14). Briefly, the purified MBP-Parkin (20 μg of MBP-Parkin/ml) was incubated in a reaction buffer (50

* This work was supported by grants-in-aid from the Ministry of Education, Culture, Sports, Science and Technology of Japan (to K. T.). The costs of publication of this article were defrayed in part by the payment of page charges. This article must therefore be hereby marked "*advertisement*" in accordance with 18 U.S.C. Section 1734 solely to indicate this fact.

[S] The on-line version of this article (available at http://www.jbc.org) contains supplemental Table 1 and Fig. 1.

[1] To whom correspondence should be addressed. Tel. and Fax: +81-3-3823-2237; E-mail: tanakak@rinshoken.or.jp.

[2] The abbreviations used are: PD, Parkinson disease; E1, ubiquitin-activating enzyme; E2, ubiquitin-conjugating enzyme; E3, ubiquitin ligase; GST, glutathione *S*-transferase; MBP, maltose-binding protein.

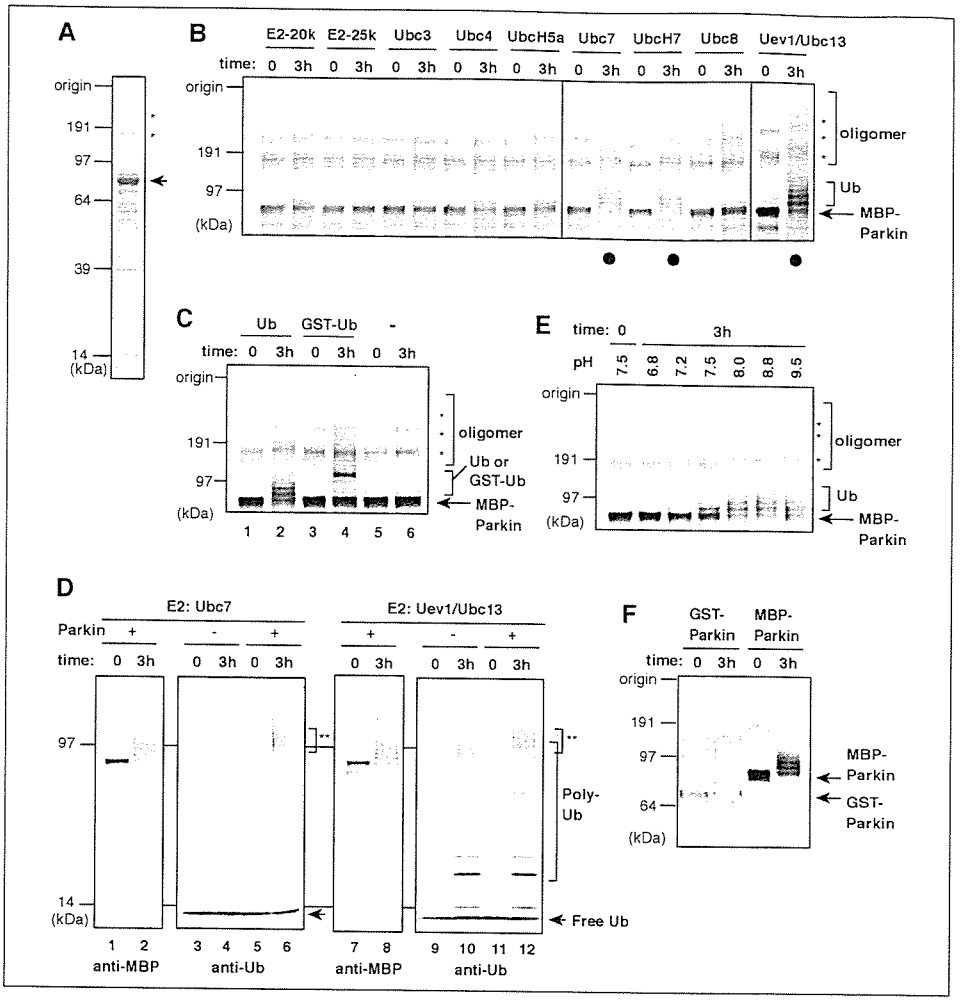

FIGURE 1. ***In vitro* ubiquitylation assay using Parkin derived from *E. coli*.** *A*, purified MBP-Parkin was visualized by CBB staining. The *arrow* indicates MBP-Parkin, and the *asterisks* indicate oligomerization bands. *B*, MBP-Parkin catalyzes autoubiquitylation in cooperation with Ubc7, UbcH7, and Uev1-Ubc13 (*solid circles*). MBP-Parkin was subjected to *in vitro* ubiquitylation assay and to immunoblotting with anti-MBP antibody. *Ub*, ladders derived from autoubiquitylation, *, oligomerization bands. *C*, confirmation of autoubiquitylation of MBP-Parkin. To demonstrate that the slower migrating ladders are because of autoubiquitylation, a reconstitution assay was repeated in the absence (−) or presence of ubiquitin (*Ub*) or GST-ubiquitin (*GST-Ub*). *D*, the high molecular weight forms of MBP-Parkin are recognized by anti-ubiquitin antibody. *Double asterisks* indicate the signal derived from MBP-Parkin autoubiquitylation. The *arrow* indicates free ubiquitin. *E*, Parkin prefers weak alkaline conditions to exert its E3 activity. *F*, GST-Parkin rarely exhibits E3 activity. Bacterial recombinant GST- and MBP-Parkin were concurrently subjected to ubiquitylation assay. Ubc7 was used as E2 in *C*, *E*, and *F*. Anti-MBP antibody was used in *B*, *C*, and *E*, and anti-Parkin antibody was used in *F*.

mM Tris-HCl, pH 8.8, 2 mM dithiothreitol, 5 mM $MgCl_2$, and 4 mM ATP) with 50 μg of ubiquitin/ml (Sigma), 1.6 μg of recombinant mouse E1/ml and 20 μg of purified E2 or 100 μg of various E2-expressing *E. coli* lysate/ml at 32 °C for 2 h and subjected to immunoblotting with anti-MBP antibody (New England BioLabs), anti-parkin (1A1) antibody (15), or anti-ubiquitin antibody (DakoCytomation, Carpinteria, CA). In some cases, GST-ubiquitin or methylated ubiquitin (BostonBiochem, Cambridge, MA) was used instead of native ubiquitin. The subsequent thrombin cleavage was performed by incubation on ice for 3 h in the presence of thrombin and 2 mM $CaCl_2$.

RESULTS

Autoubiquitylation by MBP-Parkin Fusion Protein—In 2001, Rankin *et al.* (16) reported that glutathione *S*-transferase (GST)-tagged Parkin purified from *E. coli* possesses E3 activity. However, we found that the E3 activity of this GST-Parkin is very weak (Fig. 1*F*), and thus there is a need for a more sensitive E3 assay system for bacterially expressed recombinant Parkin. During studies of other RING finger proteins, we recognized the superiority of the MBP-tag relative to GST-tag in purifying RING finger proteins that retain their E3 activities (12, 13, 17, 18) and hence decided to use MBP-Parkin. MBP-Parkin was purified using a modified *E. coli* strain BL21(DE3) codon-plus-RIL (Fig. 1*A*) and then incubated with ATP, ubiquitin, E1, and one of the E2 enzymes indicated in Fig. 1*B*, and we subjected it to immunoblotting with anti-MBP antibody. High molecular mass ladders derived from autoubiquitylation (see below) were observed when MBP-Parkin was incubated with Ubc7, UbcH7, and Uev1-Ubc13 (Fig. 1*B*, highlighted by the *solid circles*). Note that the slower migrating bands of more than 160 kDa observed even at reaction time zero (Fig. 1*B*, *asterisks*) or without ubiquitin (Fig. 1, *A* and *C*, *asterisks*) are derived from MBP-Parkin oligomerization. To test whether the modification acquired by MBP-Parkin is due to ubiquitylation, the same reaction products were subjected to immunoblotting with anti-ubiquitin antibody. When Ubc7 was used as E2 (Fig. 1*D*, *lanes 1–6*), only modified MBP-Parkin was detected by anti-ubiquitin antibody (*lane 6*, *double asterisks*), indicating that the modification acquired by MBP-Parkin was indeed autoubiquitylation. When Uev1-Ubc13 was used, a polyubiquitylation signal was observed even in the absence of MBP-Parkin (Fig. 1*D*, *lanes 9* and *10*), because Uev1-Ubc13 complex itself can catalyze polyubiquitin chain formation (19). Also in this case, modified MBP-Parkin reacted with anti-ubiquitin antibody, confirming the above conclusion (see Fig. 1*D*, *double asterisks* in *lane 12*; note that the difference between *lanes 10* and *12* corresponds to the autoubiquitylation signal of MBP-Parkin). Moreover, the replacement of ubiquitin with GST-ubiquitin retarded the mobility of these ladders (Fig. 1*C*, *lanes 3* and *4*), and the exclusion of ubiquitin completely quenched such ladders (Fig. 1*C*, *lanes 5* and *6*). Based on these results, we concluded that MBP-Parkin catalyzes autoubiquitylation in cooperation with Ubc7, UbcH7, and Uev1-Ubc13. Interestingly, autoubiquitylation became evident when the pH of the reaction buffer was increased to 8.0 and 8.8, indicating that Parkin prefers weak alkaline conditions to exhibit its E3 activity *in vitro* (Fig. 1*E*). Because MBP-Parkin possesses stronger E3

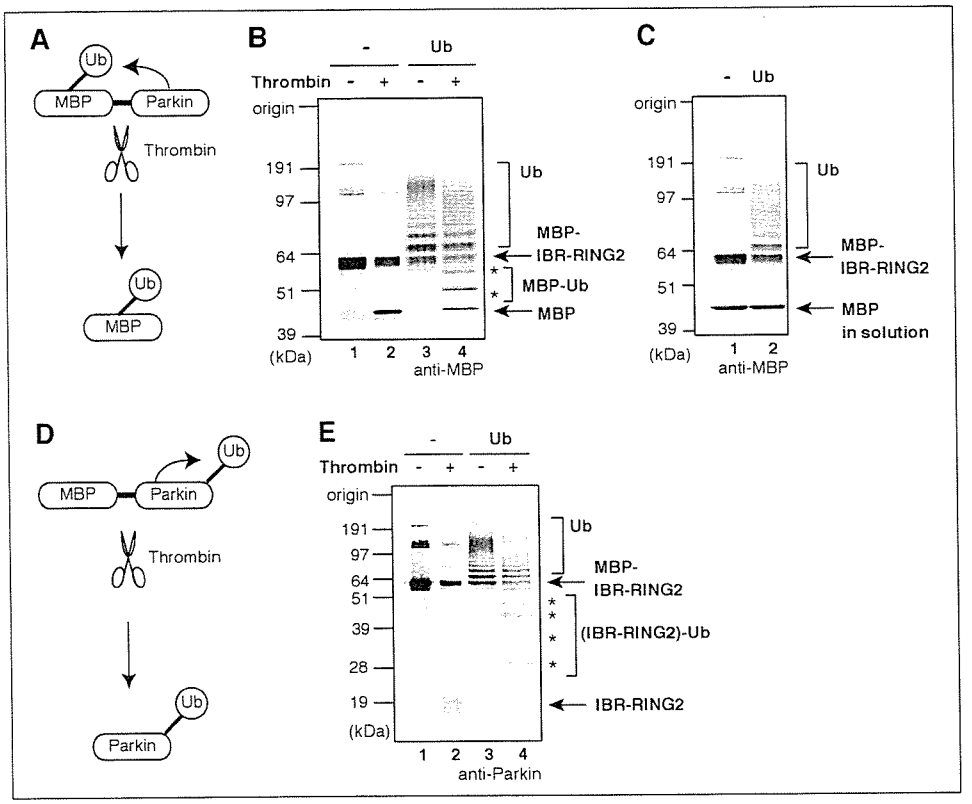

FIGURE 2. **In-frame-fused MBP can be a good pseudosubstrate of Parkin.** *A*, a schematic diagram of Parkin catalyzed ubiquitylation of MBP. If the MBP portion is ubiquitylated, a change in its mobility would be recognized by immunoblotting after cleavage. *B*, the MBP-(IBR-RING2) fused protein (see Fig. 4) was subjected to *in vitro* ubiquitylation, subsequent cleavage into MBP moiety, and immunoblotting with anti-MBP antibody. The MBP portion of IBR-RING2 was ubiquitylated (*asterisks*). *C*, MBP can be ubiquitylated only when it is in the physical vicinity of Parkin. Note that free MBP in solution was not ubiquitylated. *D*, a schematic diagram of Parkin-catalyzed autoubiquitylation. *E*, IBR-RING2 portion is also ubiquitylated. *Asterisks* in *lane 4* show the ubiquitylated IBR-RING2 moiety (compare *lane 4* with *2*). Ubc7 was used as E2 in these experiments.

activity than GST-Parkin, as shown in Fig. 1*F*, we used MBP-Parkin in the following experiments.

Fused MBP Is a Good Pseudo-substrate to Monitor E3 Activity of Parkin—We next determined whether the MBP portion or Parkin portion (or both) is ubiquitylated. To check this, we purified MBP-LVPRGS-Parkin, in which a thrombin-digestion sequence is inserted between MBP and Parkin. As depicted in Fig. 2*A*, if the MBP moiety is ubiquitylated, its molecular weight would increase by ubiquitylation and subsequent digestion, but if not ubiquitylated, its molecular weight would remain unchanged. First we tried to split MBP-LVPRGS-Parkin by thrombin; however, this recombinant protein was hardly digested for some unknown reason (data not shown). We next fused the C-terminal IBR-RING2 region of Parkin to MBP-LVPRGS (hereafter dubbed IBR-RING2, see Fig. 4*A*), and this construct was cleaved moderately (Fig. 2*B*, *lanes 1* and *2*). When IBR-RING2 was subjected to an ubiquitylation assay and subsequently separated into MBP and IBR-RING2 portions by thrombin digestion, the molecular weight of MBP moiety was clearly increased (see the *asterisks* in Fig. 2*B*, *lanes 3* and *4*), meaning that the MBP portion is ubiquitylated. Does this result mean that bacterial MBP protein is the substrate for Parkin? The answer is no. When sole MBP protein was incubated with IBR-RING2, this free MBP was not ubiquitylated at all, even though IBR-RING2 was autoubiquitylated as described (Fig. 2, compare *C* with *B*). This result indicates that the IBR-RING2 region of Parkin ubiquitylates fused-MBP, but not unbound MBP, and strongly suggests that Parkin recognizes MBP as a substrate not because of its amino acid sequence but because of its physical vicinity to Parkin. As depicted in Fig. 2*D*, when the same experiment was repeated using an anti-Parkin antibody, the molecular weight of the IBR-RING2 moiety was also increased meaning that both MBP and IBR-RING2 portions were ubiquitylated (Fig. 2*E*). Although many putative substrates of Parkin have been reported, the lack of a good *in vitro* substrate makes any biochemical study difficult. Our study revealed that fused MBP could be a good pseudo-substrate to monitor the E3 activity of Parkin.

Parkin by Itself Catalyzes Multiple Monoubiquitylation—The Uev1-Ubc13 heterodimer is an E2 involved in the formation of Lys-63-linked polyubiquitylation (19). We confirmed that our Uev1-Ubc13 complex is functional (Fig. 1*D* and supplemental Fig. 1*A*). Motivated by the findings that Parkin catalyzes Lys-63-linked polyubiquitylation (20, 21) and Parkin cooperates with Uev1-Ubc13 in our assay (Fig. 1*B*), we investigated the mode of Parkin-catalyzed ubiquitylation. Parkin could either catalyze multiple monoubiquitylation, Lys-48-linked polyubiquitylation, or Lys-63-linked polyubiquitylation. Lys-48-linked polyubiquitylation has been studied most and it essentially directs the substrate to degradation by the proteasome. In contrast, the Lys-63-linked polyubiquitylation and monoubiquitylation serve as a signal other than proteasomal-proteolysis (22–24). We first used methylated ubiquitin (hereafter referred to as Met-Ub) in which all lysine residues are blocked by methylation and is incapable of polyubiquitylation. If Parkin catalyzes polyubiquitylation, the use of Met-Ub would shorten the ladder of ubiquitylation but if not, the ubiquitylation pattern would remain unchanged. Unexpectedly, the use of Met-Ub and Uev1-Ubc13 did not change the ubiquitylation pattern, indicating that Parkin catalyzes multiple monoubiquitylation *in vitro* (Fig. 3*A*). The same result was observed when Ubc7 was used as E2 (Fig. 3*B*), and these results were more evident when IBR-RING2 (Fig. 4*A*) was utilized (Fig. 3, *C* and *D*). Repeated experiments using lysine-less ubiquitin, in which all lysine residues were changed to arginine, showed it cannot form a polyubiquitin chain, again confirmed the consequence (Fig. 3*E*). It is noteworthy that sole Ubc13 itself assisted autoubiquitylation of Parkin as well as the Uev1-Ubc13 complex (supplemental Fig. 1*B*), again supporting this conclusion. These results allowed us to conclude that the mode of ubiquitylation catalyzed by intrinsic Parkin *in vitro* is multiple monoubiquitylation rather than polyubiquitylation (see "Discussion").

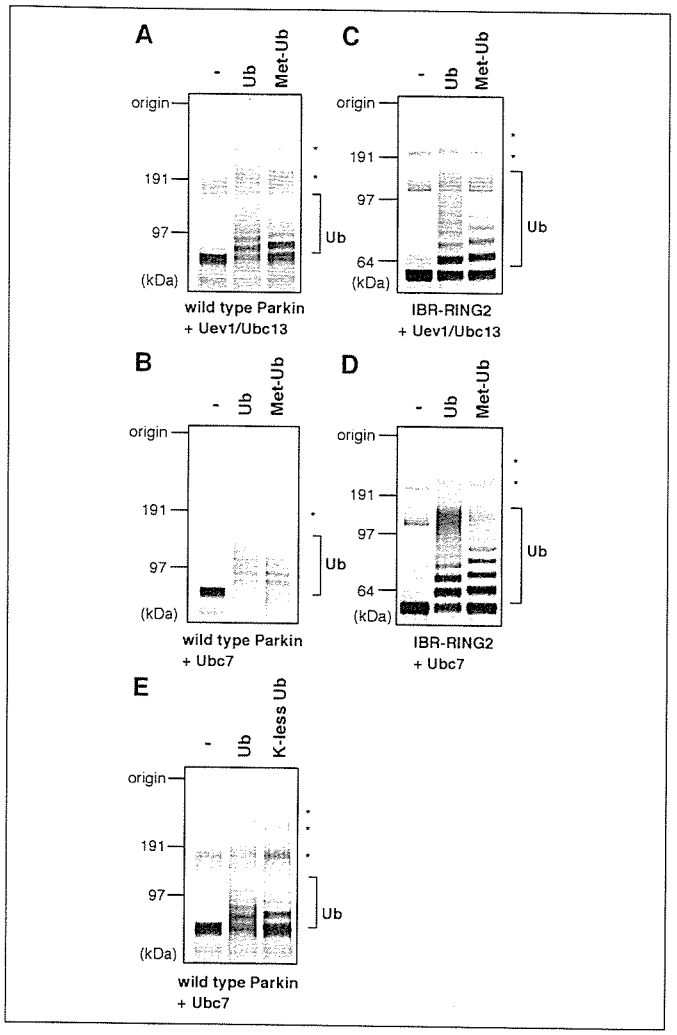

FIGURE 3. **Parkin catalyzes multiple monoubiquitylation.** *A* and *B*, *in vitro* ubiquitylation assay was performed in the absence (−) or presence of ubiquitin (*Ub*) or methylated-ubiquitin (*Met-Ub*; cannot form polyubiquitylation chain). Uev1-Ubc13 was used as E2 in *A* and Ubc7 in *B*. Almost identical ubiquitylation patterns were observed in Ub and Met-Ub, indicating that Parkin catalyzes multiple monoubiquitylation. *C* and *D*, the result was more evident when IBR-RING2 (see Fig. 4) was utilized. Uev1-Ubc13 was used as E2 in *C* and Ubc7 in *D*. *E*, the same experiment was performed using lysine-less ubiquitin. *Ub*, autoubiquitylation; *, oligomerization bands. Anti-MBP antibody was used in all experiments.

Mode of E3 Activity of Parkin with Pathogenic Missense Mutations—At present, dozens of disease-relevant mutations of Parkin have been reported, and the primary cause of autosomal recessive juvenile parkinsonism is assumed to be impairment of the E3 activity of Parkin by such mutations. However, it is still contentious whether Parkin with PD-causing mutation loses its E3 activity or not (see supplemental Table 1), primarily because of the absence of a sensitive E3-activity assay system using recombinant Parkin. To settle this problem, we examined the E3 activity of MBP-Parkin harboring various mutations and deletions. Three in-frame exonic deletions and 19 PD-linked mutations distributed throughout Parkin were selected (Fig. 4*A*). In addition, two Parkin species, one lacks its Ubl domain (ΔUbl) and the other possesses only C-terminally IBR-RING2 domain (IBR-RING2), were also generated. When these MBP-Parkin mutants were incubated with Ubc7 as E2, only mutations neighboring the second RING finger motif (Fig. 4*A*, *solid circles*) abolished the E3 activity completely (Fig. 4*B*). A nonsense mutation lacking the rear RING finger motif had no E3 activity and sole IBR-RING2 retained the E3 activity (Fig. 4, *light gray circles*), indicating that the second RING finger motif is the catalytic core for the E3 activity of Parkin. Contrary to what was assumed, all disease-relevant mutations other than those in RING2 still possessed E3 activities equivalent to that of the wild-type Parkin (Fig. 4*B*). The same results were observed when UbcH7 or Uev1-Ubc13 was used as E2 (data not shown). In these assays, we used a bacterially expressed recombinant Parkin, and to our knowledge, this is the first direct evidence that E3 activity of the strictly pure Parkin harboring various pathogenic mutations is not compromised.

DISCUSSION

To date, numerous biochemical studies have been performed to understand the E3 activity of Parkin. However, it is difficult to rule out the possible involvement of other E3s (see Introduction). Furthermore, the lack of a good model substrate spurs the difficulty to check the intrinsic E3 activity of Parkin. We thus set up a sensitive E3 assay system using bacterially expressed recombinant Parkin. Our assay system has some advantages; namely, we can obtain a large quantity of MBP-Parkin with higher E3 activity than GST-Parkin (Fig. 1). In addition, this fusion protein was already primed for ubiquitylation even in the absence of model substrate, because fused MBP can work as a good pseudo-substrate (Fig. 2). More importantly, because MBP-Parkin is purified from *E. coli*, it is free from possible contamination of other E3(s). The establishment of this assay allowed us to perform a thorough biochemical characterization of Parkin protein.

Interestingly, sole Parkin catalyzes multiple monoubiquitylation *in vitro* (Fig. 3). Moreover, although Doss-Pepe *et al.* (20) reported that Parkin accelerates polyubiquitin chain formation, the MBP-Parkin in our assay did not stimulate the assembly of polyubiquitin chain (Fig. 1*D*, compare *lanes 4* and *6*, and *10* and *12*, respectively). These results seemingly suggest that the ubiquitylation catalyzed by Parkin functions not for proteasomal degradation but for non-proteasomal-proteolytic function(s), such as transcriptional regulation and/or membrane trafficking *in vivo*. However, it is still premature to make such conclusion. Although we showed that pure Parkin catalyzes multiple monoubiquitylation *in vitro* (Fig. 3), some additional factor(s) like E4 can work together *in vivo*, and this needs to be considered. E4 can extend the ubiquitin chain by recognizing the ubiquitin moiety of a ubiquitylated-protein as a substrate (25). If such an E4-like factor(s) cooperates with Parkin *in vivo*, it is still possible that monoubiquitylation catalyzed by Parkin is used as the scaffold for further polyubiquitylation and finally functions for proteasomal degradation. All things considered, further studies are obviously required; in particular, the authentic substrate and the function of Parkin-catalyzed ubiquitylation need to be addressed.

Another unexpected result was that most of the PD-relevant missense mutations do not abrogate E3 activity of Parkin (Fig. 4). Only missense mutations in the rear RING finger motif abolished the E3 activity, revealing that not the first but the second RING finger motif is the catalytic core of Parkin. Recently, several studies that focused on the pathophysiological mechanisms of Parkin have been published (26–30). Although our results on enzymatic activities of mutant Parkin are not fully consistent with previous reports (see supplemental Table 1), methodological differences in the E3 assay may account for the conflicting observation. For example, in one study immunoprecipitated Parkin was used as the source of E3 *in vitro* (31) and in other studies, E3 activity of Parkin was checked by whether or not coexpression of Parkin in cells enhances the ubiquitylation of the putative substrate (7, 30). Although there is little discrepancy, recent studies and our present work drew the same conclusion that the dysfunction of Parkin is not simply attributable to catalytic impairment of its E3 activity. Indeed, several missense mutations cause Parkin to be sequestered into an aggresome-like structure, and this phenomenon may be involved in disease pathogenesis

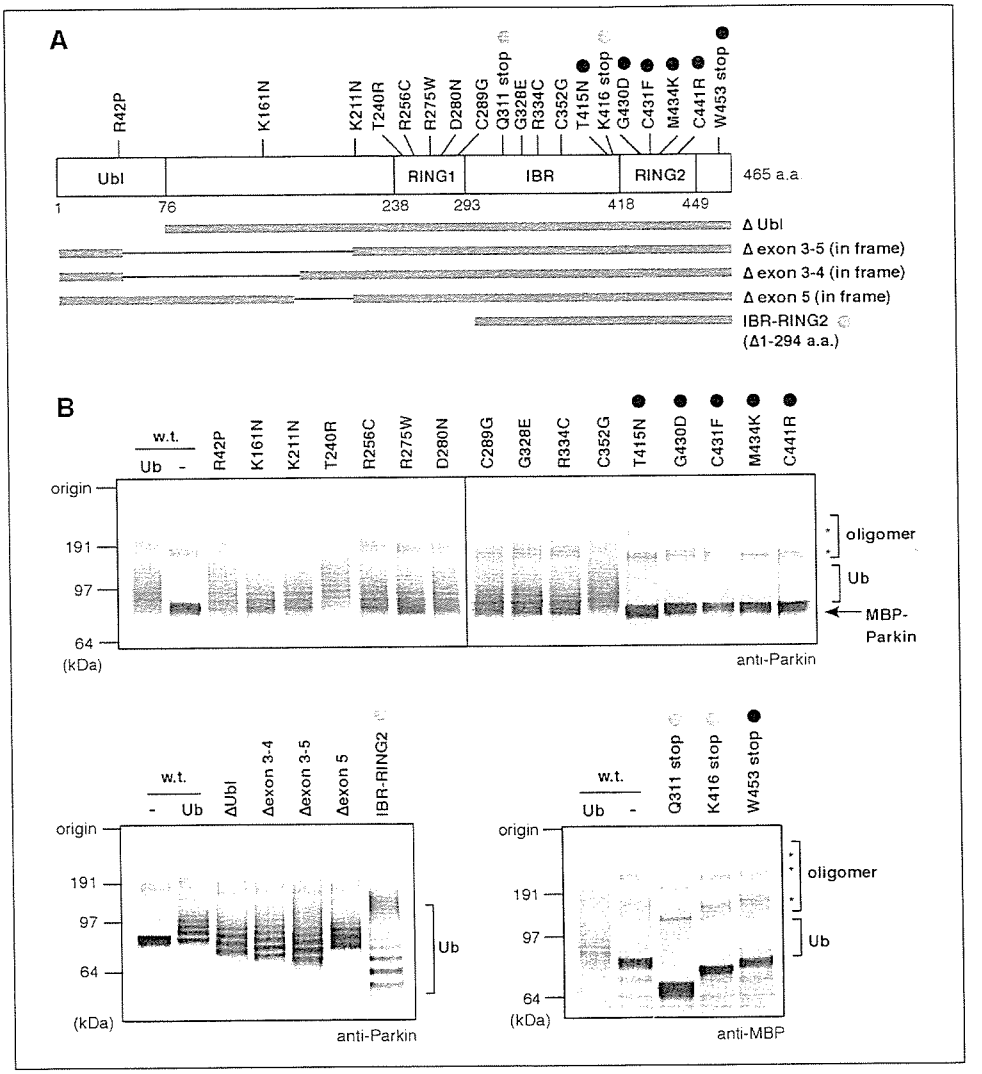

FIGURE 4. *A*, schematic diagram of disease-relevant mutations and exonic deletions of Parkin. *B*, E3 activities of various Parkin proteins bearing PD-linked mutations and deletions. Note that mutations neighboring the second RING finger motif (*solid circles*) abolished E3 activity of Parkin. *Light gray circles* indicate that the RING2 is the catalytic core of Parkin (see text for details). Conversely, pathogenic mutants other than RING2 mutants retain E3 activities equivalent to that of the wild-type (*w.t.*) control. *Ub*, autoubiquitylation; *, oligomerization bands.

(27–30). We think that disease-relevant mutations cause not only attenuation of E3 activity but also a variety of primary defects such as sequestration into aggresome and dissociation from its partner protein, and possibly a complex of such defects may eventually lead to Parkin dysfunction and autosomal recessive juvenile parkinsonism.

PD is the second most prevalent neurodegenerative disorder, and thus, analysis of Parkin is important in terms of public welfare. Indeed, a large number of articles on Parkin have been published; however, because of fierce scientific competition, not all Parkin-related phenomena were critically scrutinized although there remains room for close examination. For example, Pawlyk *et al.* (32) recently inspected the anti-Parkin antibodies and uncovered a high non-specificity of the available Parkin antibodies. This also holds true for the E3 activity of Parkin, because precedent works could not exclude the possible involvement of another E3(s). Herein we investigated thoroughly the enzymatic activity of bacterially expressed recombinant Parkin. Although our work is not conspicuous, we hope that our biochemical characterization using pure Parkin would be a solid cornerstone for further studies, as the preceding works were.

Acknowledgments—We thank Dr. Tsunehiro Mizushima of Nagoya University for providing recombinant Ubc7 protein. We also thank all members of Prof. K. Tanaka laboratory for the helpful discussions.

REFERENCES

1. Moore, D. J., West, A. B., Dawson, V. L., and Dawson, T. M. (2005) *Annu. Rev. Neurosci.* **28**, 57–87
2. Giasson, B. I., and Lee, V. M. (2003) *Cell* **114**, 1–8
3. Ross, C. A., and Pickart, C. M. (2004) *Trends Cell Biol.* **14**, 703–711
4. Tanaka, K., Suzuki, T., Hattori, N., and Mizuno, Y. (2004) *Biochim. Biophys. Acta* **1695**, 235–247
5. Hattori, N., and Mizuno, Y. (2004) *Lancet* **364**, 722–724
6. Lohmann, E., Periquet, M., Bonifati, V., Wood, N. W., De Michele, G., Bonnet, A. M., Fraix, V., Broussolle, E., Horstink, M. W., Vidailhet, M., Verpillat, P., Gasser, T., Nicholl, D., Teive, H., Raskin, S., Rascol, O., Destee, A., Ruberg, M., Gasparini, F., Meco, G., Agid, Y., Durr, A., and Brice, A. (2003) *Ann. Neurol.* **54**, 176–185
7. Ren, Y., Zhao, J., and Feng, J. (2003) *J. Neurosci.* **23**, 3316–3324
8. Corti, O., Hampe, C., Koutnikova, H., Darios, F., Jacquier, S., Prigent, A., Robinson, J. C., Pradier, L., Ruberg, M., Mirande, M., Hirsch, E., Rooney, T., Fournier, A., and Brice, A. (2003) *Hum. Mol. Genet.* **12**, 1427–1437
9. Imai, Y., Soda, M., Hatakeyama, S., Akagi, T., Hashikawa, T., Nakayama, K. I., and Takahashi, R. (2002) *Mol. Cell* **10**, 55–67
10. Zhong, L., Tan, Y., Zhou, A., Yu, Q., and Zhou, J. (2005) *J. Biol. Chem.* **280**, 9425–9430
11. You, J., Cohen, R. E., and Pickart, C. M. (1999) *BioTechniques* **27**, 950–954
12. Matsuda, N., Suzuki, T., Tanaka, K., and Nakano, A. (2001) *J. Cell Sci.* **114**, 1949–1957
13. Imai, N., Matsuda, N., Tanaka, K., Nakano, A., Matsumoto, S., and Kang, W. (2003) *J. Virol.* **77**, 923–930
14. Matsuda, N., Azuma, K., Saijo, M., Iemura, S., Hioki, Y., Natsume, T., Chiba, T., Tanaka, K., and Tanaka, K. (2005) *DNA Repair (Amst.)* **4**, 537–545
15. Shimura, H., Hattori, N., Kubo, S., Yoshikawa, M., Kitada, T., Matsumine, H., Asakawa, S., Minoshima, S., Yamamura, Y., Shimizu, N., and Mizuno, Y. (1999) *Ann.*

Neurol. **45,** 668–672
16. Rankin, C. A., Joazeiro, C. A., Floor, E., and Hunter, T. (2001) *J. Biomed. Sci.* **8,** 421–429
17. Araki, K., Kawamura, M., Suzuki, T., Matsuda, N., Kanbe, D., Ishii, K., Ichikawa, T., Kumanishi, T., Chiba, T., Tanaka, K., and Nawa, H. (2003) *J. Neurochem.* **86,** 749–762
18. Takai, R., Matsuda, N., Nakano, A., Hasegawa, K., Akimoto, C., Shibuya, N., and Minami, E. (2002) *Plant J.* **30,** 447–455
19. Hofmann, R. M., and Pickart, C. M. (1999) *Cell* **96,** 645–653
20. Doss-Pepe, E. W., Chen, L., and Madura, K. (2005) *J. Biol. Chem.* **280,** 16619–16624
21. Lim, K. L., Chew, K. C., Tan, J. M., Wang, C., Chung, K. K., Zhang, Y., Tanaka, Y., Smith, W., Engelender, S., Ross, C. A., Dawson, V. L., and Dawson, T. M. (2005) *J. Neurosci.* **25,** 2002–2009
22. Chen, Z. J. (2005) *Nat. Cell Biol.* **7,** 758–765
23. Hicke, L. (2001) *Nat. Rev. Mol. Cell Biol.* **2,** 195–201
24. Pickart, C. M. (2000) *Trends Biochem. Sci.* **25,** 544–548
25. Richly, H., Rape, M., Braun, S., Rumpf, S., Hoege, C., and Jentsch, S. (2005) *Cell* **120,** 73–84
26. Cookson, M. R., Lockhart, P. J., McLendon, C., O'Farrell, C., Schlossmacher, M., and Farrer, M. J. (2003) *Hum. Mol. Genet.* **12,** 2957–2965
27. Gu, W. J., Corti, O., Araujo, F., Hampe, C., Jacquier, S., Lucking, C. B., Abbas, N., Duyckaerts, C., Rooney, T., Pradier, L., Ruberg, M., and Brice, A. (2003) *Neurobiol. Dis.* **14,** 357–364
28. Henn, I. H., Gostner, J. M., Lackner, P., Tatzelt, J., and Winklhofer, K. F. (2005) *J. Neurochem.* **92,** 114–122
29. Wang, C., Tan, J. M., Ho, M. W., Zaiden, N., Wong, S. H., Chew, C. L., Eng, P. W., Lim, T. M., Dawson, T. M., and Lim, K. L. (2005) *J. Neurochem.* **93,** 422–431
30. Sriram, S. R., Li, X., Ko, H. S., Chung, K. K., Wong, E., Lim, K. L., Dawson, V. L., and Dawson, T. M. (2005) *Hum. Mol. Genet.* **14,** 2571–2586
31. Staropoli, J. F., McDermott, C., Martinat, C., Schulman, B., Demireva, E., and Abeliovich, A. (2003) *Neuron* **37,** 735–749
32. Pawlyk, A. C., Giasson, B. I., Sampathu, D. M., Perez, F. A., Lim, K. L., Dawson, V. L., Dawson, T. M., Palmiter, R. D., Trojanowski, J. Q., and Lee, V. M. (2003) *J. Biol. Chem.* **278,** 48120–48128

Vol 441|15 June 2006|doi:10.1038/nature04723

LETTERS

Loss of autophagy in the central nervous system causes neurodegeneration in mice

Masaaki Komatsu[1,2]*, Satoshi Waguri[3]*†, Tomoki Chiba[1], Shigeo Murata[1], Jun-ichi Iwata[1,2], Isei Tanida[2], Takashi Ueno[2], Masato Koike[3], Yasuo Uchiyama[3], Eiki Kominami[2] & Keiji Tanaka[1]

Protein quality-control, especially the removal of proteins with aberrant structures, has an important role in maintaining the homeostasis of non-dividing neural cells[1]. In addition to the ubiquitin–proteasome system, emerging evidence points to the importance of autophagy—the bulk protein degradation pathway involved in starvation-induced and constitutive protein turnover—in the protein quality-control process[2,3]. However, little is known about the precise roles of autophagy in neurons. Here we report that loss of *Atg7* (autophagy-related 7), a gene essential for autophagy, leads to neurodegeneration. We found that mice lacking *Atg7* specifically in the central nervous system showed behavioural defects, including abnormal limb-clasping reflexes and a reduction in coordinated movement, and died within 28 weeks of birth. *Atg7* deficiency caused massive neuronal loss in the cerebral and cerebellar cortices. Notably, polyubiquitinated proteins accumulated in autophagy-deficient neurons as inclusion bodies, which increased in size and number with ageing. There was, however, no obvious alteration in proteasome function. Our results indicate that autophagy is essential for the survival of neural cells, and that impairment of autophagy is implicated in the pathogenesis of neurodegenerative disorders involving ubiquitin-containing inclusion bodies.

Macroautophagy (hereafter referred to as autophagy) is an evolutionarily conserved pathway in which the cytoplasm and organelles are engulfed within double-membraned vesicles, known as autophagosomes, in preparation for the turnover and recycling of these cellular constituents[4]. Genetic studies using various model organisms have highlighted the importance of autophagy in physiological and pathological events[5]. The principal role of autophagy is in the supply of nutrients for survival, as shown in yeast[6] and early neonatal mice[7,8]. Autophagy also has a role in cellular remodelling during differentiation and the development of multicellular organisms, such as dauer formation in *Caenorhabditis elegans*[9] and metamorphosis in *Drosophila melanogaster*[10]. Moreover, constitutive autophagy, which occurs independently of nutrient stress, contributes to mouse liver homeostasis[8], major histocompatibility class (MHC) II antigen presentation[11], and cellular defence against invading streptococci[12] and *Mycobacterium tuberculosis*[13]. However, the physiological functions of autophagy, particularly in neurons, are still largely unknown.

To examine the relationship between neuronal pathology and autophagy deficiency *in vivo*, we crossed *Atg7*-conditional knockout mice ($Atg7^{flox/flox}$) (ref. 8) with transgenic mice expressing Cre recombinase under the control of the nestin promoter (nestin-*Cre*) (ref. 14), to produce mice deficient for *Atg7* specifically in the central nervous system ($Atg7^{flox/flox}$; nestin-*Cre*). Atg7 is an E1-like enzyme for both the Atg12- and Atg8-conjugation systems[15], and is essential

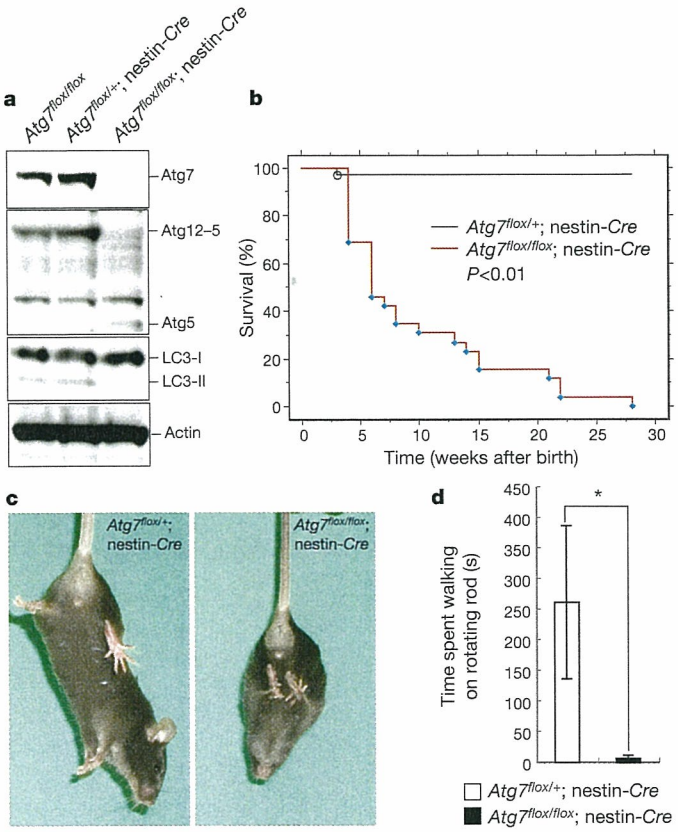

Figure 1 | Behavioural disorder in $Atg7^{flox/flox}$; nestin-*Cre* mice. **a**, Impairment of two ATG-conjugation systems (Atg12 and LC3) in the Atg7-deficient brain. Brain homogenates from P28 mice were immunoblotted with antibodies against Atg7, Atg5 and LC3. Actin was used as a loading control. Data shown are representative of three separate experiments. **b**, Kaplan–Meier survival curves of $Atg7^{flox/+}$; nestin-*Cre* ($n = 41$) and $Atg7^{flox/flox}$; nestin-*Cre* ($n = 26$) mice over 28 weeks. **c**, Abnormal limb-clasping reflexes in $Atg7^{flox/flox}$; nestin-*Cre* mice at P28. When lifted by the tail, $Atg7^{flox/+}$; nestin-*Cre* mice behave normally, extending their hind limbs and bodies. In contrast, $Atg7^{flox/flox}$; nestin-*Cre* mice bend their legs towards their trunk or tighten their back limbs to their bodies and anterior limbs. **d**, Movement ataxia in $Atg7^{flox/flox}$; nestin-*Cre* mice at P28. Motor coordination was tested using a rotarod assay. $Atg7^{flox/+}$; nestin-*Cre* ($n = 5$) and $Atg7^{flox/flox}$; nestin-*Cre* ($n = 5$) mice were placed on a rod rotating at 20 r.p.m., and the time spent on the rod was counted. Data show mean ± s.d. *, $P < 0.01$ (Student's *t*-test). There was no significant sex difference in survival rate and onset-stage of abnormal limb-clasping and tremor in $Atg7^{flox/flox}$; nestin-*Cre* mice.

[1]Laboratory of Frontier Science, Tokyo Metropolitan Institute of Medical Science, Bunkyo-ku, Tokyo 113-8613, Japan. [2]Department of Biochemistry, Juntendo University School of Medicine, Bunkyo-ku, Tokyo 113-8421, Japan. [3]Department of Cell Biology and Neurosciences, Osaka University Graduate School of Medicine, Osaka 565-0871, Japan. †Present address: Department of Anatomy and Histology, Fukushima Medical University School of Medicine, 1 Hikarigaoka, Fukushima 960-1295, Japan.
*These authors contributed equally to this work.

for autophagy[8]. Atg7 protein was absent at postnatal day (P)28 in brain from *Atg7*$^{flox/flox}$; nestin-*Cre* but not control (*Atg7*$^{flox/+}$; nestin-*Cre*) mice (Fig. 1a). The level of Atg7 protein in other tissues such as liver, lung, heart and muscle was comparable between *Atg7*$^{flox/flox}$; nestin-*Cre* and control mice (data not shown). Atg12–Atg5 conjugate was detected only in the brains of control mice by immunoblotting with an anti-Atg5 antibody (Fig. 1a). In contrast, free Atg5, which was faintly observed in the control mouse brain, was clearly increased in the mutant brain (Fig. 1a). The mammalian homologue of yeast Atg8, microtubule-associated protein 1 light-chain 3 (LC3), exists in two forms (LC3-I and LC3-II)[16]. Both forms were detected in brains from control mice, but only the LC3-I form was detected in *Atg7*$^{flox/flox}$; nestin-*Cre* brain (Fig. 1a). The loss of both Atg7 and LC3-II proteins was observed from P0 in the brain of *Atg7*$^{flox/flox}$; nestin-*Cre* mice (Supplementary Fig. S1). These results indicate complete impairment of autophagy in the central nervous system of *Atg7*$^{flox/flox}$; nestin-*Cre* mice after birth.

Atg7$^{flox/flox}$; nestin-*Cre* mice were viable at birth and indistinguishable in appearance from their littermates. However, the survival rate of the mutant mice diminished markedly by four weeks after birth, and all *Atg7*$^{flox/flox}$; nestin-*Cre* mice were dead within 28 weeks (Fig. 1b). We also observed growth retardation as early as P14 in these mice (data not shown). Furthermore, the mice showed motor and behavioural deficits, including abnormal limb-clasping reflexes (Fig. 1c) and tremor, and in some cases, they walked on their tiptoes. In a rotarod test, most *Atg7*$^{flox/flox}$; nestin-*Cre* mice fell after grasping the rod only briefly (Fig. 1d). These motor and behavioural deficits began to appear at P14–P21. These results suggest that autophagy deficiency in the central nervous system results in a severe neurological disorder.

Histological analysis using Meyer's haematoxylin and eosin (H&E) staining showed marked atrophy of the cerebral cortical region of *Atg7*$^{flox/flox}$; nestin-*Cre* brain at P56 (Fig. 2a, b). The ratios of cortical thickness to dorsoventral thickness of the brain in *Atg7*$^{flox/+}$; nestin-*Cre* and *Atg7*$^{flox/flox}$; nestin-*Cre* mice were 0.17 ± 0.00031 and 0.15 ± 0.00034, respectively ($n = 5$, $P < 0.01$). Notably, almost no large pyramidal neurons were observed in *Atg7*$^{flox/flox}$; nestin-*Cre* mice compared with the corresponding region in brains from control mice (Fig. 2c, d). Immunostaining for the glial marker GFAP (glial fibrillary acidic protein) showed an increase in GFAP signal in the cerebral cortex of *Atg7*$^{flox/flox}$; nestin-*Cre* mice (Fig. 2e, f), suggesting the presence of neuronal damage in this region. In the cerebellar

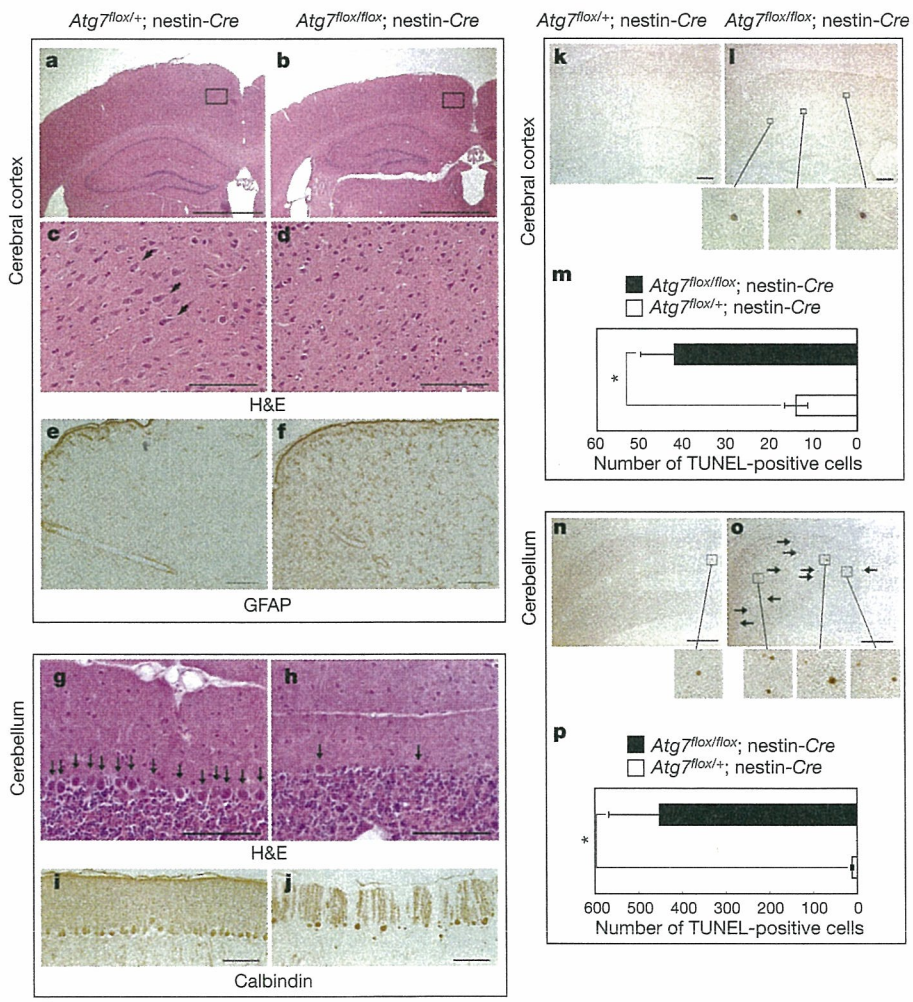

Figure 2 | Marked cell death in autophagy-deficient cerebral cortex and cerebellum. **a–f**, Histological analyses of *Atg7*$^{flox/+}$; nestin-*Cre* (left) and *Atg7*$^{flox/flox}$; nestin-*Cre* (right) cerebral cortex at P56. Cryosections were stained with H&E (**a–d**) or immunostained for the glial marker GFAP (**e**, **f**). Boxed areas in **a** and **b** are magnified in **c** and **d**, respectively. Arrows in **c** point to large pyramidal neurons in the cerebral cortex. **g–j**, Histological analysis of *Atg7*$^{flox/+}$; nestin-*Cre* (left) and *Atg7*$^{flox/flox}$; nestin-*Cre* (right) cerebellum at P56. Cryosections were stained with H&E (**g**, **h**) or immunostained for the Purkinje marker calbindin (**i**, **j**). Arrows in **g** and **h** indicate cerebellar Purkinje cells. **k–p**, TUNEL staining of the cerebral cortex (**k**, **l**) and cerebellum (**n**, **o**) at P56 in *Atg7*$^{flox/+}$; nestin-*Cre* (**k**, **n**) and *Atg7*$^{flox/flox}$; nestin-*Cre* (**l**, **o**) sections. TUNEL-positive cells are indicated with arrows and shown as higher magnification images beneath panels **l**, **n** and **o**. Histograms show the average number (±s.d.) of TUNEL-positive cells in ten sections for three animals of each genotype (**m**, **p**). *, $P < 0.05$ (*t*-test). Scale bars, 1 mm (**a**, **b**), 100 μm (**c–j**), 250 μm (**k**, **l**, **n**, **o**). We observed no sex difference in brain morphology or neuronal loss in *Atg7*$^{flox/flox}$; nestin-*Cre* mice.

cortex, H&E staining revealed a large reduction in the number of Purkinje cells in the mutant brain (Fig. 2g, h), which was further confirmed by immunolabelling of Purkinje cells with an anti-calbindin antibody (Fig. 2i, j). Similar neuronal loss was also recognized in the hippocampal pyramidal cell layer of mutant brain (Supplementary Fig. S2).

To determine whether the reduced number of neurons observed in *Atg7*$^{flox/flox}$; nestin-*Cre* mouse brain was caused by cell death, we performed TUNEL (TdT-mediated dUTP nick end labelling) assays. We observed a marked increase in the number of TUNEL-positive cells in the cerebral cortex (Fig. 2k–m) and granular cell layer of the cerebellum at P56 in *Atg7*$^{flox/flox}$; nestin-*Cre* mice (Fig. 2n–p) compared with control mouse brains. Although loss of Purkinje cells was observed in the mutant brain, we could not detect TUNEL-positive Purkinje cells at any developmental stage examined. However, when *Atg7* was specifically depleted in Purkinje cells using transgenic mice expressing Cre recombinase under the control of the *Pcp2* gene promoter (Pcp2-*Cre*), a marked reduction in the number of Purkinje cells was detected in the absence of TUNEL reactivity (data not shown), suggesting that neurons deficient in autophagy can die in a cell-autonomous fashion. Together, these results indicate that lack of autophagy in the central nervous system leads to neurodegeneration.

We have previously reported that autophagy is responsible for constitutive protein turnover in quiescent hepatocytes even under nutrient-rich conditions, and that a defect in autophagy leads to the accumulation of large, ubiquitin-containing inclusion bodies[8]. We therefore probed brain sections with an anti-ubiquitin antibody to examine the presence of ubiquitin-containing inclusion bodies. At P56, ubiquitin-positive dots were detected in several regions of the *Atg7*$^{flox/flox}$; nestin-*Cre* mouse brain, including the cerebral cortex (Fig. 3b), cerebellar Purkinje cells (Fig. 3d), hippocampal pyramidal neurons (Fig. 3f), thalamus (data not shown), hypothalamus (Fig. 3h), amygdala (Fig. 3j) and pontine nuclei (Fig. 3l). The degree of staining varied by region. For example, whereas most neuronal

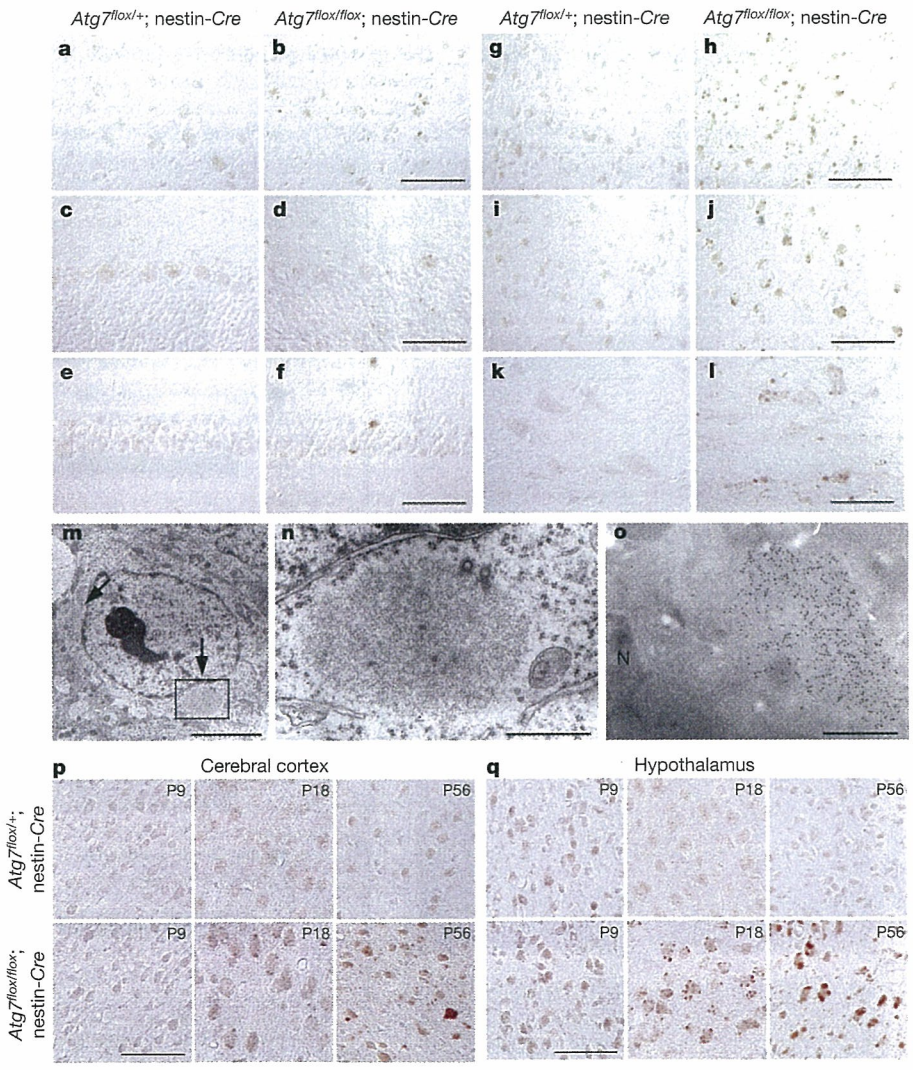

Figure 3 | Appearance of ubiquitin-positive inclusions in autophagy-deficient neurons. a–l, The presence of ubiquitin-positive dots was examined immunohistochemically in several regions including cerebral cortex (**a**, **b**), cerebellum (**c**, **d**), hippocampus (**e**, **f**), hypothalamus (**g**, **h**), amygdala (**i**, **j**) and pontine nuclei (**k**, **l**) of *Atg7*$^{flox/+}$; nestin-*Cre* and *Atg7*$^{flox/flox}$; nestin-*Cre* mice. Note the presence of numerous ubiquitin dots in the amygdala and hypothalamus of the representative mutants. Scale bars, 50 μm. **m**, **n**, Electron micrographs of the brain of *Atg7*$^{flox/flox}$; nestin-*Cre* mice. Inclusion bodies (arrows) were often observed in *Atg7*$^{flox/flox}$; nestin-*Cre* hypothalamus. The boxed region in **m** is shown in **n**. Inclusion bodies were not detected in *Atg7*$^{flox/+}$; nestin-*Cre* brain (data not shown). Scale bars, 5 μm (**m**), 1 μm (**n**). **o**, Immunoelectron micrograph of ubiquitin in a representative *Atg7*$^{flox/flox}$; nestin-*Cre* hypothalamus. N, nucleus. Scale bar, 1 μm. **p**, **q**, Immunohistochemical detection of ubiquitin-positive inclusions in the cerebral cortex (**p**) and hypothalamus (**q**) at P9, P18 and P56. Brain sections of each genotype at the indicated ages were immunostained with an anti-ubiquitin antibody. Ubiquitin-positive inclusions appeared at P18 and became larger with ageing in the brain of *Atg7*$^{flox/flox}$; nestin-*Cre* mice. Scale bars, 50 μm.

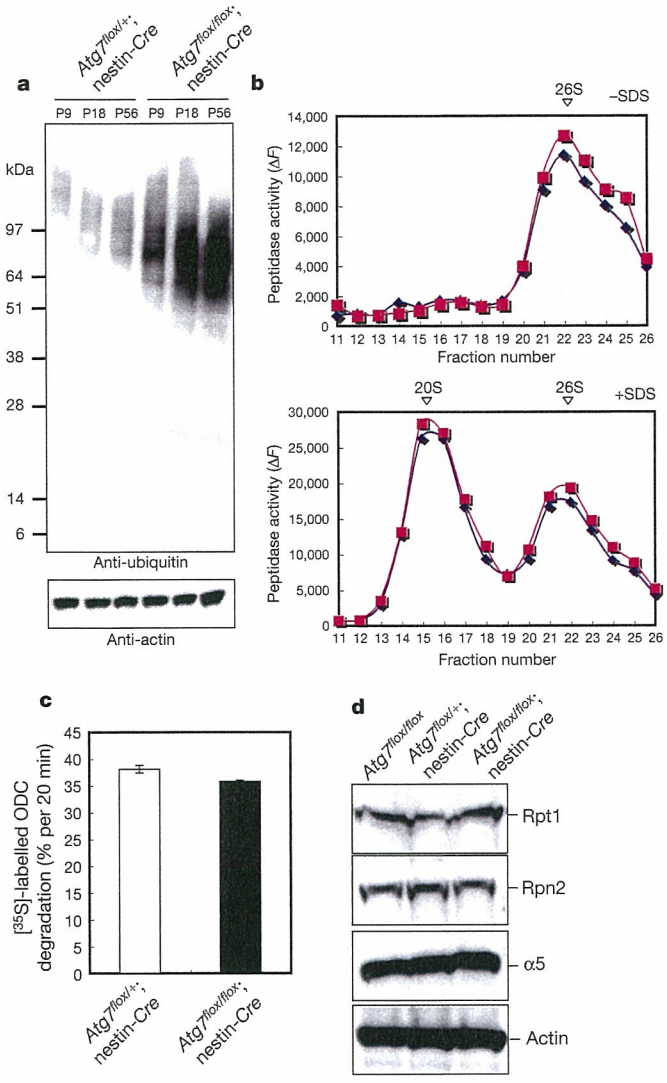

Figure 4 | Qualitative and quantitative analyses of proteasomes in autophagy-deficient brain. **a**, Increase in ubiquitinated proteins in *Atg7*$^{flox/flox}$; nestin-*Cre* mouse brain over time. Homogenates of P9, P18 and P56 brains from *Atg7*$^{flox/+}$; nestin-*Cre* and *Atg7*$^{flox/flox}$; nestin-*Cre* mice were immunoblotted with an anti-ubiquitin antibody. An anti-actin antibody was used as a loading control. Data shown are representative of three separate experiments. We observed no sex difference in the accumulation of ubiquitin in *Atg7*$^{flox/flox}$; nestin-*Cre* mice. **b**, Peptide hydrolysis activity of 20S and 26S proteasomes. Homogenates from P28 *Atg7*$^{flox/+}$; nestin-*Cre* (blue) and *Atg7*$^{flox/flox}$; nestin-*Cre* (pink) brains were fractionated by glycerol density gradient centrifugation (10–40% glycerol from fraction 1 to fraction 30). Aliquots from each fraction were used for the assay of chymotryptic activity of proteasomes using Suc-LLVY-AMC as a substrate in the absence (top) or presence (bottom) of 0.05% SDS. The sedimenting positions of 20S and 26S proteasomes are indicated with arrowheads. Note that whereas 26S proteasomes exist in active forms in tissues, 20S proteasomes are latent and are activated artificially by a low concentration of SDS. **c**, ATP-dependent degradation of [^{35}S]-labelled ODC. Degradation of [^{35}S]-labelled ODC was assayed using crude extracts from P28 *Atg7*$^{flox/+}$; nestin-*Cre* and *Atg7*$^{flox/flox}$; nestin-*Cre* brains. The experiment was repeated three times, and values represent mean ± s.d. In the above assays, there were no significant differences between *Atg7*$^{flox/+}$; nestin-*Cre* and *Atg7*$^{flox/flox}$; nestin-*Cre* mice. **d**, Immunoblot analysis of 26S proteasome components. Homogenates from P28 *Atg7*$^{flox/flox}$, *Atg7*$^{flox/+}$; nestin-*Cre* and *Atg7*$^{flox/flox}$; nestin-*Cre* brains were immunoblotted with antibodies against the indicated proteins. Data shown are representative of three separate experiments. There was no change in proteasome status for the different genotypes.

cells in the amygdala (Fig. 3j) and hypothalamus (Fig. 3h) contained several ubiquitin dots of small to large size, only a small number of cerebellar Purkinje cells stained for ubiquitin, and the immunoreactive dots were of small size (Fig. 3d). Electron microscopy showed that *Atg7*$^{flox/flox}$; nestin-*Cre* hypothalamic neurons had circular or elliptical large structures composed of fibrillar elements in the perikarya (Fig. 3m, n). Immunoelectron microscopy further confirmed that these aberrant structures contained ubiquitin (Fig. 3o). These ubiquitin dots appeared not only in the perikarya of neurons, but also in the intercellular space (see Fig. 3h, j, l). Dots found in the intercellular space might correspond to ubiquitin inside neurites, because they were observed in myelinated axons around pontine nuclei using both light and electron microscopy (Supplementary Fig. S3a, b). In contrast, almost no ubiquitin dots were observed in astroglial cells (Supplementary Fig. S3c). Together with the results in Fig. 3, we concluded that most of the distinct ubiquitin dots were located in neurons.

We examined the development of ubiquitin-containing inclusion bodies at different stages by dissecting the brains of *Atg7*$^{flox/+}$; nestin-*Cre* and *Atg7*$^{flox/flox}$; nestin-*Cre* mice at P9, P18 and P56. Only a few ubiquitin-positive aggregates were noted in the neurons of control and mutant cerebral cortex and hypothalamus at P9 (Fig. 3p, q). In contrast, several ubiquitin-containing inclusions were clearly noted in *Atg7*$^{flox/flox}$; nestin-*Cre* cortex and hypothalamus at P18, increasing in number and size by P56 (Fig. 3p, q). These results indicate an age-dependent increase in ubiquitin-containing inclusion bodies in autophagy-deficient neurons. Consistent with the above immunohistochemical analysis (Fig. 3p, q), immunoblot analysis revealed increasing levels of high-molecular-mass polyubiquitinated proteins with age in the brains of *Atg7*$^{flox/flox}$; nestin-*Cre* mice (Fig. 4a), and an increase in their insoluble forms at later developmental stages (data not shown).

Finally, we examined whether autophagy deficiency influences proteasome functions. The chymotryptic activities of 26S and 20S proteasomes (measured using Suc-LLVY-MCA as a substrate) were comparable in extracts from both control and *Atg7*$^{flox/flox}$; nestin-*Cre* brains (Fig. 4b). Furthermore, the ATP-dependent degradation of ornithine decarboxylase (ODC) by 26S proteasomes was similar in control and mutant brains (Fig. 4c). Moreover, the relative amounts of several subunits of the 26S proteasome did not change in the brain irrespective of autophagy deficiency (as detected by immunoblotting, Fig. 4d). These results indicate that age-dependent accumulation of ubiquitin-positive aggregates in the autophagy-deficient brain occurs despite the apparently normal function of proteasomes.

Over the past decade, researchers working in the field of neurodegenerative diseases have made great progress in uncovering the mechanisms of these disorders by focusing on the interplay between proteolytic stress and neural cell death[17,18]. Increasing evidence indicates that ubiquitin-positive inclusion bodies—the pathological hallmark of various neurodegenerative diseases—are formed by dysfunction of proteasome degrading machinery[3]. Indeed, proteins with aberrant structure impair proteasome functions directly, thus attenuating 'garbage disposal'[19]. On the other hand, the accumulation of autophagosomes owing to impairment of fusion with lysosomes is observed in various disorders, including Alzheimer's disease[20–22], and it has been proposed that autophagy functions to degrade toxic proteins in familial neurodegenerative diseases[23–25]. However, it remains unknown whether these two proteolytic systems work independently or cooperatively to maintain protein homeostasis in cells. Furthermore, whether autophagy has a role in cell death or cell survival is currently under debate[26].

We have shown that *Atg7*$^{flox/flox}$; nestin-*Cre* mice exhibit neurological abnormalities and neuronal death, suggesting that impaired autophagy causes neurodegeneration. We suggest a particularly important role for autophagy in the brain, to which nutrients must be constantly supplied from other organs, even under fasting conditions. Moreover, we find that autophagy deficiency in neurons leads to the accumulation of ubiquitin-containing inclusion bodies,

without obvious deficits in proteasome function. Hence, our data indicate a central role for constitutive autophagy in the elimination of unfavourable proteins and in the survival of neurons, independent of the proteasome system (see the proposed model in Supplementary Fig. S4). Although we do not know whether autophagy and proteasome degradation target a similar set of normal and/or misfolded proteins, it is plausible that the autophagic pathway assists in degrading accumulated intractable proteins when cellular levels of aberrant proteins overwhelm the disposal capacity of the proteasome.

We have shown that a lack of autophagy is associated with neurodegeneration, even in the absence of harmful gene products found in neurodegenerative disorders such as Huntington's disease, Parkinson's disease and amyotrophic lateral sclerosis. We therefore predict that the role of autophagy becomes even more critical in the pathogenesis of such neurodegenerative diseases, when disease-related, aggregation-prone proteins are expressed as a result of genetic mutations and/or environmental insults, leading to early-onset symptoms.

METHODS

Animals. Nestin-*Cre* transgenic mice[14] were purchased from the Jackson Laboratory. $Atg7^{flox/flox}$ mice[8] were bred with nestin-*Cre* transgenic mice to produce $Atg7^{flox/flox}$; nestin-*Cre* mice. Mice were housed in a pathogen-free facility. Motor function was assessed using a rotarod test[27]. Experimental protocols were approved by the Ethics Review Committee for Animal Experimentation at the Tokyo Metropolitan Institute of Medical Science.

Immunoblot analysis. Immunoblots were carried out as described previously[8]. Antibodies against Atg7, Atg5 and LC3 have been described previously[8]. Antibodies against Rpt1, Rpn2 and α5 were provided by K. B. Hendil. Polyclonal anti-ubiquitin (FK2; Medical & Biological Laboratories) and anti-actin (MAB1501R; Chemicon) antibodies were also used.

Histological examination. $Atg7^{flox/+}$; nestin-*Cre* and $Atg7^{flox/flox}$; nestin-*Cre* mice were fixed by cardiac perfusion with 0.1 M phosphate buffer containing 4% paraformaldehyde, 4% sucrose for light microscopy and immunohistochemistry, with 0.1 M phosphate buffer containing 2% paraformaldehyde, 2% glutaraldehyde for standard electron microscopy, or with 0.1 M phosphate buffer containing 4% paraformaldehyde, 0.1% glutaraldehyde for immunoelectron microscopy. Brain tissues were excised and processed for morphological analysis as described previously[8,28]. For light microscopic analysis, 10-μm cryosections were cut and stained with H&E or immunolabelled with the following antibodies: anti-human NeuN (Abcam), anti-GFAP (Sigma), anti-calbindin (Sigma), anti-myelin basic protein (MBP; MCA409S, Serotec) and anti-ubiquitin (DAKO) antibodies. The TUNEL assay has been described previously[28]. For counting TUNEL-positive signals in the cerebral cortex, 60 coronal sections containing the anterior portion of the hippocampus (~0.6-mm thick in total) were cut, and TUNEL staining was performed on every sixth section, on a total of ten sections.

Electron microscopy and immunoelectron microscopy. Fixed brains were post-fixed with 1% OsO_4, embedded in Epon812 and sectioned. Immunoelectron microscopy was carried out on cryothin sections as described previously[29]. In brief, brains were frozen in phosphate buffer containing 2.3 M sucrose and 20% polyvinyl pyrrhoridon. Ultrathin sections were mounted on Formvar carbon-coated nickel grids, blocked with 1% bovine serum albumin (BSA) in PBS, and incubated with anti-ubiquitin antibody (1B3) and colloidal gold-conjugated secondary antibody.

Glycerol gradient analysis. Samples were fractionated by 10–40% (v/v) linear glycerol density gradient centrifugation (22 h, 100,000*g*) as described previously[30].

Assay of proteasome activity. Peptidase activity was measured using a fluorescent peptide substrate, succinyl-Leu-Leu-Val-Tyr-7-amido-4-methylcoumarin (Suc-LLVY-MCA), as described previously[30]. Ornithine decarboxylase (ODC)-degradation activity was assayed as described previously[30].

Received 6 February; accepted 20 March 2006.
Published online 19 April 2006.

1. Forman, M. S., Trojanowski, J. Q. & Lee, V. M. Neurodegenerative diseases: a decade of discoveries paves the way for therapeutic breakthroughs. *Nature Med.* 10, 1055–1063 (2004).
2. Shintani, T. & Klionsky, D. J. Autophagy in health and disease: a double-edged sword. *Science* 306, 990–995 (2004).
3. Goldberg, A. L. Protein degradation and protection against misfolded or damaged proteins. *Nature* 426, 895–899 (2003).
4. Reggiori, F. & Klionsky, D. J. Autophagosomes: biogenesis from scratch? *Curr. Opin. Cell Biol.* 17, 415–422 (2005).
5. Levine, B. & Klionsky, D. J. Development by self-digestion: molecular mechanisms and biological functions of autophagy. *Dev. Cell* 6, 463–477 (2004).
6. Tsukada, M. & Ohsumi, Y. Isolation and characterization of autophagy-defective mutants of *Saccharomyces cerevisiae*. *FEBS Lett.* 333, 169–174 (1993).
7. Kuma, A. *et al.* The role of autophagy during the early neonatal starvation period. *Nature* 432, 1032–1036 (2004).
8. Komatsu, M. *et al.* Impairment of starvation-induced and constitutive autophagy in *Atg7*-deficient mice. *J. Cell Biol.* 169, 425–434 (2005).
9. Melendez, A. *et al.* Autophagy genes are essential for dauer development and life-span extension in *C. elegans*. *Science* 301, 1387–1391 (2003).
10. Juhasz, G., Csikos, G., Sinka, R., Erdelyi, M. & Sass, M. The *Drosophila* homolog of Aut1 is essential for autophagy and development. *FEBS Lett.* 543, 154–158 (2003).
11. Paludan, C. *et al.* Endogenous MHC class II processing of a viral nuclear antigen after autophagy. *Science* 307, 593–596 (2005).
12. Nakagawa, I. *et al.* Autophagy defends cells against invading group A *Streptococcus*. *Science* 306, 1037–1040 (2004).
13. Gutierrez, M. G. *et al.* Autophagy is a defense mechanism inhibiting BCG and *Mycobacterium tuberculosis* survival in infected macrophages. *Cell* 119, 753–766 (2004).
14. Betz, U. A., Vosshenrich, C. A., Rajewsky, K. & Muller, W. Bypass of lethality with mosaic mice generated by Cre–*loxP*-mediated recombination. *Curr. Biol.* 6, 1307–1316 (1996).
15. Ohsumi, Y. Molecular dissection of autophagy: two ubiquitin-like systems. *Nature Rev. Mol. Cell Biol.* 2, 211–216 (2001).
16. Kabeya, Y. *et al.* LC3, a mammalian homologue of yeast Apg8p, is localized in autophagosome membranes after processing. *EMBO J.* 19, 5720–5728 (2000).
17. Ciechanover, A. & Brundin, P. The ubiquitin proteasome system in neurodegenerative diseases: sometimes the chicken, sometimes the egg. *Neuron* 40, 427–446 (2003).
18. Bossy-Wetzel, E., Schwarzenbacher, R. & Lipton, S. A. Molecular pathways to neurodegeneration. *Nature Med.* 10 (Suppl.), S2–S9 (2004).
19. Bence, N. F., Sampat, R. M. & Kopito, R. R. Impairment of the ubiquitin–proteasome system by protein aggregation. *Science* 292, 1552–1555 (2001).
20. Yu, W. H. *et al.* Macroautophagy–a novel β-amyloid peptide-generating pathway activated in Alzheimer's disease. *J. Cell Biol.* 171, 87–98 (2005).
21. Tanaka, Y. *et al.* Accumulation of autophagic vacuoles and cardiomyopathy in LAMP-2-deficient mice. *Nature* 406, 902–906 (2000).
22. Nishino, I. *et al.* Primary LAMP-2 deficiency causes X-linked vacuolar cardiomyopathy and myopathy (Danon disease). *Nature* 406, 906–910 (2000).
23. Webb, J. L., Ravikumar, B., Atkins, J., Skepper, J. N. & Rubinsztein, D. C. α-Synuclein is degraded by both autophagy and the proteasome. *J. Biol. Chem.* 278, 25009–25013 (2003).
24. Ravikumar, B. *et al.* Inhibition of mTOR induces autophagy and reduces toxicity of polyglutamine expansions in fly and mouse models of Huntington disease. *Nature Genet.* 36, 585–595 (2004).
25. Fortun, J., Dunn, W. A. Jr, Joy, S., Li, J. & Notterpek, L. Emerging role for autophagy in the removal of aggresomes in Schwann cells. *J. Neurosci.* 23, 10672–10680 (2003).
26. Levine, B. & Yuan, J. Autophagy in cell death: an innocent convict? *J. Clin. Invest.* 115, 2679–2688 (2005).
27. Bontekoe, C. J. *et al.* Knockout mouse model for *Fxr2*: a model for mental retardation. *Hum. Mol. Genet.* 11, 487–498 (2002).
28. Koike, M. *et al.* Involvement of two different cell death pathways in retinal atrophy of cathepsin D-deficient mice. *Mol. Cell. Neurosci.* 22, 146–161 (2003).
29. Waguri, S. *et al.* Cysteine proteinases in GH4C1 cells, a rat pituitary tumour cell line, are secreted by the constitutive and regulated secretory pathways. *Eur. J. Cell Biol.* 67, 308–318 (1995).
30. Tanahashi, N. *et al.* Hybrid proteasomes. Induction by interferon-γ and contribution to ATP-dependent proteolysis. *J. Biol. Chem.* 275, 14336–14345 (2000).

Supplementary Information is linked to the online version of the paper at www.nature.com/nature.

Acknowledgements We thank T. Kaneko, T. Kouno and K. Tatsumi for technical assistance. We also thank A. Yabashi, K. Kanno, F. Kaji and K. Ikeue for help with morphological analysis, J. Ezaki for discussion, and Z. Yue for critical reading of the manuscript. This work was supported in part by a Grant-in-Aid from the Ministry of Education, Culture, Sports, Science and Technology of Japan.

Author contributions M.K. and T.C. generated $Atg7^{flox/flox}$ mice, and M.K. and J.I. performed most of the experiments to characterize $Atg7^{flox/flox}$; nestin-*Cre* mice. S.W. performed histological and microscopic analyses, and S.M. performed the biochemical analysis of proteasome activity. M.K., S.W. and K.T. wrote the paper. All authors discussed the results and commented on the manuscript.

Author Information Reprints and permissions information is available at npg.nature.com/reprintsandpermissions. The authors declare no competing financial interests. Correspondence and requests for materials should be addressed to K.T. (tanakak@rinshoken.or.jp).